



Implementation and validation of a new irrigation scheme in the ISBA land surface model

Arsène Druel^{1,2}, Simon Munier¹, Anthony Mucia¹, Clément Albergel^{1,3} and Jean-Christophe Calvet¹

¹CNRM, Université de Toulouse, Météo-France, CNRS, Toulouse, France

5 ²Now at Ecologie des Forêts Méditerranéennes (URFM), Institut national de recherche pour l'agriculture, l'alimentation et l'environnement (INRAE), Avignon, France

³Now at European Space Agency Climate Office, ECSAT, Harwell Campus, OX11 0FD Didcot, Oxfordshire, United Kingdom

10 *Correspondence to:* Jean-Christophe Calvet (jean-christophe.calvet@meteo.fr), Arsène Druel (arsene.druel@umr-cnrm.fr)

Abstract. With an increase in the number of natural processes represented, global land surface models (LSMs) have become more and more accurate in representing natural terrestrial ecosystems. However, they are still limited, especially in the representation of the impact of agriculture on land surface variables. This is particularly true for agro-hydrological processes related to a strong human control on freshwater. While most LSMs consider natural processes only, the development of human-related processes, e.g. crop phenology and irrigation in LSMs, is key. In this study we present the implementation of a new irrigation scheme in the ISBA (Interaction between Soil, Biosphere, and Atmosphere) LSM. This highly flexible scheme is designed to account for various configurations and can be applied at different spatial scales. For each vegetation type within a model grid cell, three irrigation systems can be used at the same time. A limited number of parameters are used to control (1) the amount of water used for irrigation, (2) irrigation triggering (based on the soil moisture stress) and (3) crop seasonality (emergence, harvesting). After a presentation of the simulations of the new scheme at a plot scale, an evaluation is proposed over Nebraska (USA). This region is chosen for its high irrigation density and because independent observations of irrigation practices can be used to verify the simulated irrigation amounts. The ISBA simulations with and without the irrigation scheme are compared to different satellite-based observations. The comparison shows that the irrigation scheme improves the simulated vegetation variables such as leaf area index and gross primary productivity and other variables largely impacted by irrigation such as evapotranspiration and land surface temperature.

15
20
25



In addition to a better representation of land surface processes, the results point to potential applications
30 of this new version of the ISBA model for water resource monitoring and climate change impact
studies.

1 Introduction

Amongst the global water withdrawal from rivers, reservoirs and groundwater, the share used for
agriculture is estimated to reach 69 % on average, with some regional heterogeneity - over 90 % in
35 some regions (Hoekstra and Mekonnen, 2012, FAO, 2014). This amount of water is likely to increase in
the future in relation to climate warming and population growth (United Nations et al., 2019, Field et
al., 2014). Future irrigation needs will likely be stronger in Africa. Now, only 5 % of cultivated land is
under irrigation in Africa, against 21 % at a global scale (FAO, 2014). The historical evolution of
irrigation also points to increasing water consumption: the area equipped for irrigation nearly doubled
40 from 1900 to 1950, when it tripled from 1950 to 2005 (Siebert et al., 2015).

Irrigation is used to increase crop yields by controlling the soil water stress (Fraiture et al.,
2007). Several studies indicate that yields can be higher by a factor of two or more when the fields are
irrigated (Bruinsma, 2009; Colaizzi et al., 2009; Siebert and Döll, 2010; FAO, 2014). However,
freshwater is already a limited resource and the current evolution of irrigation has a substantial impact
45 on: (1) river discharge, with a decrease in their lower reaches due to diversions and impoundments for
irrigation (Tang et al., 2008; Piao et al., 2010; Grafton et al., 2018), (2) groundwater level, with critical
low levels observed in case of intensive irrigation (Rodell et al., 2009; Döll et al., 2012; Pfeiffer and
Lin, 2014), (3) the surface energy budget through an increase of evapotranspiration, which can lead to
surface cooling (Kueppers et al., 2007; Lobell et al., 2008; Jiang et al., 2014). Water vapour originating
50 from large scale irrigation water supply can be recycled to rainfall and affect non-irrigated areas (Moore
and Rojstaczer, 2002; DeAngelis et al., 2010; Carrillo-Guerrero et al., 2013; Harding et al., 2013). It can
also affect the dynamics of the monsoon (Douglas et al., 2006; Saeed et al., 2009; Shukla et al., 2014)
and influence climate at both regional and global scales (Sacks et al., 2009; Puma and Cook, 2010).
These findings show a gradual and significant influence of changes in irrigated areas on the



55 hydrological cycle (e.g. Adegoke et al., 2003; Haddeland et al., 2006; Rost et al., 2008; Döll et al.,
2009; Hanasaki et al., 2010; Biemans et al., 2011). The ability of numerical models to reproduce these
different impacts and feedbacks is thus essential in order to understand the role of irrigation in the Earth
climate system at different spatial scales (Zaitchik et al., 2005). Representing irrigation could
potentially improve weather and climate forecast skill (Ozdogan et al., 2010). However, as presented
60 below, irrigation is generally represented in models in a too simplistic way.

Land surface models (LSMs) represent land surface biophysical processes and variables,
including soil moisture and vegetation biomass, in a way that is fully consistent with the representation
of carbon, water and energy fluxes. However, current models have to improve the representation of
anthropogenic factors and their interactions with natural processes (Verburg et al., 2016). In particular,
65 LSMs need to represent the complexity of irrigation practices as much as possible, and their impact on
the environment. However, as highlighted by Chukalla et al. (2015), most of the large scale LSMs
currently represent only one type of irrigated vegetation (mostly C4 crops, i.e. crops with a C4
photosynthesis carbon fixation type, such as corn, sorghum), with only one type of irrigation practice
(e.g. sprinkling or flooding), one season per year and no inter-annual variability of vegetation density.
70 Among others, this is the case in the current version of the ISBA (Interaction between Soil, Biosphere,
and Atmosphere; Noilhan and Planton, 1989) LSM, with C4 crops irrigated with sprinkling (Voirin-
Morel, 2003; Calvet et al., 2008). In reality, there is a lot of different vegetation types which can be
irrigated, from orchards to pastures (FAO, 2014), and different irrigation techniques with different ways
to apply water (above the vegetation or directly on the ground for sprinkling and flooding irrigation
75 techniques, respectively). The type of irrigation is recognised to change (1) the irrigation efficiency
(Evans and Sadler, 2008), (2) the amount of freshwater used for irrigation per surface unit (FAO, 2014),
and (3) the impact of irrigation on water resources (Khan and Abbas, 2007). Moreover, some
specificities of irrigation such as the timing and frequency of water application can affect the ecosystem
and atmospheric responses to irrigation (Sorooshian et al., 2012). Some models include a representation
80 of irrigation without having an interactive vegetation scheme and using climatological values instead
(such as with the LSI-Noah model, a NASA land information system and LSM combination, use in



Lawston et al., 2015), thereby precluding inter-annual variability of vegetation density and the impact of irrigation on vegetation growth. Having a more complete irrigation description is needed to follow the irrigation seasonality, and to represent possible changes in crop phenology such as emergence and
85 harvest dates. The impact of changing irrigation characteristics in a context of climate change could thereby be evaluated, such as increasing irrigation efficiency (currently around 56%; FAO, 2014) and freshwater saving potential (Perry et al., 2017; Koech and Langat, 2018).

The objective of this work is to develop and evaluate a more detailed representation of irrigation practices into the ISBA LSM within the SURFEX (SURFace EXternalisée) modelling platform
90 (Masson et al., 2013). In SURFEX, land cover is described by ECOCLIMAP-II (Faroux et al., 2013). This study takes advantage of the ECOCLIMAP-SG (Calvet and Champeaux, 2020; Supplement S1) major update of ECOCLIMAP-II. While the SURFEX framework allows the coupling of terrestrial processes with atmospheric and hydrological models, only offline ISBA simulations are considered in this study.

95 The evaluation of the new irrigation scheme is made over the state of Nebraska (United States of America, USA). This area presents a high density of irrigated fields (Fig. 1) and large freely available observational datasets for evaluation.

Section 2 presents the observational datasets, the current version of the ISBA LSM, the description of the new irrigation scheme, followed by a description of the validation protocol. Section 3
100 illustrates the impact of the new irrigation scheme when compared to a model run without irrigation. An evaluation of the performance of the model is made over Nebraska. Section 4 discusses the added value and the limits of the newly implemented irrigation scheme. Finally, section 5 presents the conclusions and future research directions.



2 Materials and Methods

105 2.1 Data

2.1.1 Irrigation map

One of the main challenges of this study was to obtain an upgraded map of irrigation at the global scale, to be consistent with the resolution ($300\text{ m} \times 300\text{ m}$) of the European Space Agency - Climate Change Initiative (ESA-CCI) land cover map used in ECOCLIMAP-SG. The $1\text{ km} \times 1\text{ km}$ resolution global
110 irrigation map proposed by Meier et al. (2018), based on a statistical approach and satellite data, was used. A reason to choose this product was that its development process was based (amongst other) on the ESA-CCI land cover product (v1.6.1), the same as the one used to develop the ECOCLIMAP-SG vegetation map (Supplement S1).

In order to transfer the Meier irrigation map ($1\text{ km} \times 1\text{ km}$) to ECOCLIMAP-SG ($300\text{ m} \times 300$
115 m), a spatial rescaling of the Meier map was performed. A simple majority rule was used by assigning to each $300\text{ m} \times 300\text{ m}$ grid point of ECOCLIMAP-SG the irrigation status (irrigated or rainfed) of the main corresponding grid-cell of the Meier $1\text{ km} \times 1\text{ km}$ map. An irrigation map at a spatial resolution of $300\text{ m} \times 300\text{ m}$ was obtained, with a single vegetation type attributed to each grid cell together with the irrigation status. The main limitation of this map is that there is no information on the type of irrigation.
120 In this study, we considered that all irrigation is of “sprinkler” type as this is the most common irrigation type in the USA (AQUASTAT and FAO, 2019), where the testbed area of this study is located. This entails that irrigation water is added to the precipitation forcing over the irrigated agricultural parcels.

2.1.2 Atmospheric forcing

125 The simulations presented in this study were not coupled with the atmosphere. They were forced by a simulated atmospheric dataset of the European Centre for Medium-Range Weather Forecasts (ECMWF): the ERA-5 atmospheric reanalysis at $0.25^\circ \times 0.25^\circ$ (Hersbach and Dee, 2016). This global dataset was successfully used to force the ISBA LSM in previous studies (e.g. Albergel et al., 2019, Bonan et al., 2020). Beck et al. (2019) showed that the ERA-5 precipitation dataset is reasonably



130 consistent with gauge-radar data over CONUS, except for mountainous areas. A subset of the ERA-5
forcing over Nebraska was used for the time period from 1979 to 2018. The following atmospheric
variables were used to force the ISBA LSM and were taken from ERA-5 at an hourly time step: air
temperature, wind speed, air specific humidity, atmospheric pressure, shortwave and longwave
downwelling radiation and precipitation (liquid and solid).

135 **2.1.3 Validation datasets**

A large variety of data was used to evaluate the simulations over Nebraska. Six observation datasets
were used (Table 1): the water used for irrigation, satellite-derived Leaf Area Index (LAI), gross
primary production (GPP), evapotranspiration, land surface temperature (LST), and precipitation.

Precipitation data from the Grand Island and Lincoln weather stations (40.93°N – 98.76°W,
140 40.83°N, 96.76°W, “Gi” dot in Fig. 1e and “Li” dot in Fig. 1b, respectively) were used to evaluate the
ERA5 precipitation forcing over Nebraska.

The water use records were provided by the US Geological Survey (USGS) through the National
Water Information System (available at <https://waterdata.usgs.gov/ne/nwis/wu>, last access August
2021). Every 5 years from 1985 onward, the annual raw amount of water collected for irrigation was
145 available by county, associated to the surface area of the irrigated vegetation. This allowed us to
compute the amount of water used for irrigation per unit surface area (in mm) over the specific studied
zone in Nebraska (Fig. 1e). The USGS data we used cover the 1985-2019 time period. Because of
inconsistencies in the record for 1995, this year was not taken into account.

The simulated LAI was compared with a satellite-derived LAI product at $0.01^\circ \times 0.01^\circ$ spatial
150 resolution derived from SPOT-VGT and PROBA-V satellite data (up to May 2014, and after May 2014,
respectively) by the European Copernicus Global Land Service (CGLS). This LAI product is described
in Baret et al. (2013). We used Version 2 of this product (GEOV2). It is available every 10 days for all
simulation years. The LAI time series is available from 1999 onward. It does not cover the whole
simulation time period (1979 to 2018). The simulated GPP is compared to an upscaled estimate of GPP
155 available at 0.25° from 1980 to 2013, from the FLUXCOM project (Jung et al., 2017). The simulated
evapotranspiration is compared to the GLEAM satellite-driven model estimates of land



evapotranspiration available from 2003 to 2018 (version v3.2b, Martens et al., 2017) at a spatial resolution of $0.25^\circ \times 0.25^\circ$. Finally, the simulated LST at 12h00 (local solar time) is compared to the LST derived from geostationary meteorological satellites by CGLS at 12h00 (local solar time). This product has a spatial resolution of $0.05^\circ \times 0.05^\circ$ and is available from 2009 to 2018 (Freitas et al., 2013).

2.2 The ISBA land surface model

The ISBA model (originally described in Noilhan and Planton, 1989) is the LSM developed by the research department of Météo-France (Centre National de Recherches Météorologiques, CNRM). It is embedded into the SURFEX modelling platform (Masson et al., 2013; Voldoire et al., 2017; Le Moigne et al., 2018), and can provide initial land surface conditions to various atmospheric models (e.g. ALADIN in Fischer et al., 2005), or be forced by atmospheric conditions in offline (i.e. stand-alone) mode. In SURFEX, the evolution of land surface states (surface temperature, albedo, roughness...) and fluxes (evaporation, sensible heat, ...) is simulated for four different tiles: natural and cultivated lands (e.g. deciduous and broadleaf forests, tropical, temperate and boreal grasslands, crops, deserts, ...), urban areas, oceans and inland waters (such as lakes). The ISBA LSM is used to simulate natural and cultivated lands.

In this study, the version of ISBA including photosynthesis and temporal dynamical LAI evolution in response to environmental conditions was used (ISBA-A-gs; Calvet et al., 1998; Gibelin et al., 2006), together with the multi-layer soil hydrology scheme described in Decharme et al. (2019). Moreover, an updated land cover description was used: ECOCLIMAP-SG (see Supplement S1). The simulations were based on the SURFEX v8.1 version, which is similar to the v8.0 version (Voldoire et al., 2017), but with new technical developments (Le Moigne et al., 2018). Since this study focusses on irrigation, only the tile of natural and cultivated lands was simulated with ISBA, representing the evolution of soil (temperature and water profiles), vegetation (leaf-level and canopy-level photosynthesis, biomass, LAI and carbon fluxes), surface hydrology (runoff and drainage) and snow conditions. To represent the global-scale heterogeneity of continental natural surfaces, twenty different



surface types (hereafter referred to as “nature types”) can be used in ECOCLIMAP-SG to represent the evolution of landscapes with low vegetation, with wooded vegetation, and without vegetation.

185 2.3 Irrigation modelling concept

In this study, a pre-existing simple irrigation scheme (Calvet et al., 2008) within the ISBA LSM was upgraded to build a new version able to work at a global scale and to represent several types of irrigation practices. The new irrigation scheme is operated using the ECOCLIMAP-SG land cover classification within SURFEX. The best achievable spatial resolution of ECOCLIMAP-SG is 300 m ×
190 300 m. The irrigation can be activated for ISBA versions able to simulate interactive vegetation biomass and LAI.

2.3.1 Irrigation processes

Within ISBA, irrigation is represented by imposing an additional water flux forcing to the soil-plant system. Water is applied at a given time and over a certain period of time. A number of irrigation
195 variables need to be simulated such as the irrigation amount, the irrigation rate, the irrigation start and end times. A parsimonious approach is used in order to limit the number of parameters of the model. Table 2 lists the parameters and the values used by default in this study. Irrigation is triggered using thresholds of the simulated extractable soil moisture content. Moreover, specific crop phenology parameters such as emergence and harvest dates are used for irrigated crops. Three irrigation types are
200 considered in Lawston et al. (2015): sprinkler irrigation, flood irrigation and drip irrigation. In the new version of ISBA the same irrigation types are represented but a different modelling approach is used. In this study, the sprinkler irrigation type is used. The new irrigation algorithm is based on several steps described below.

First, it is determined whether fields within the grid cell can be irrigated, i.e. they are equipped
205 for irrigation (e.g. water supply, valves, pipes...). This information is given by the irrigation map described in section 2.1.1.

Secondly, it is checked that the vegetation growth stage is compatible with irrigation. For crops, irrigation can be triggered after the emergence and until a few days before the harvest (by default two



weeks). In practice, two dates are prescribed: emergence and harvest. This is a simple way to represent
210 specific crop phenology attributes of irrigated crops. Between these two dates, irrigation is possible.
Before the emergence and after the harvest, LAI is fixed at the model's minimum value ($LAI = 0.3 \text{ m}^2$
 m^{-2}). This new irrigation scheme is able to support up to three plant growth seasons per year. The crop
phenology parameters are not applied to wooded vegetation (trees and shrubs), and can be applied
without irrigation. Irrigation can optionally be triggered without considering any specific crop
215 phenology parameter.

The availability of resources (equipment or local water distribution) is taken into account through
a default minimum return time period between two irrigations. This default parameter value is a
constant (7 days by default) but maps of this parameter could be used when available.

Irrigation can only be triggered when vegetation growths is limited by the extractable soil
220 moisture availability. The plant water stress level is evaluated using a soil wetness index (SWI) along
the root profile. The root-zone SWI (SWI_{root_zone}) is a unitless weighted average SWI value based on the
soil volumetric water content profile ($Wc_i, \text{m}^3 \text{m}^{-3}$), the field capacity volumetric water content profile
($Wfc_i, \text{m}^3 \text{m}^{-3}$) and the wilting point profile ($Wwilt_i$, depending on clay and sand fraction, $\text{m}^3 \text{m}^{-3}$), for
each soil layer i . The root fraction inside each soil layer (f_{root_i}) is used as a weighting factor:

$$225 \quad SWI_{root_zone} = \sum_{i=1}^{n_{soil}} f_{root_i} \times \frac{Wc_i - Wwilt_i}{Wfc_i - Wwilt_i} \quad (1)$$

where n_{soil} is the number of top soil layers containing roots. This value depends on the considered
vegetation type. For example, $n_{soil} = 9$ for crops, with a rooting depth of 1.5 m.

A SWI_{root_zone} value close to one corresponds to a well-watered soil, while a value close to zero
indicates extreme stress. In order to trigger irrigation, the SWI_{root_zone} value is compared to predefined
230 SWI thresholds given as input parameters. These SWI thresholds are evolving during the irrigation
season and default values used in this study are fixed to 0.7 for the first irrigation, 0.55 for the second
irrigation, 0.4 for the third irrigation, and 0.25 afterwards (following Voirin-Morel, 2003 and Calvet et
al., 2008).

If all of these conditions are satisfied, irrigation is triggered with a predefined quantity of water
235 of 30 mm (by default), following Calvet et al. (2008). The irrigation water flux is evenly distributed



over a period of time of 8 hours (by default) and is applied on top of the vegetation canopy like precipitation for sprinkler irrigation. In this case, the irrigation water can be intercepted by vegetation and a fraction evaporates. In the case of drip or flood irrigation, the water flux is applied directly to the soil surface, with no leaf interception. In this study, only sprinkler irrigation is considered. Irrigation simulations are illustrated in Supplements S2 and S3 over southwestern France and over the Hampton irrigated area in Nebraska (Fig. 1e), respectively. Observed monthly precipitation in Nebraska is presented for contrasting years in Supplement S4.

All the values of the new parameters presented above have been set within a default configuration. These values can be user-defined for each nature type and for each grid cell, including, when possible, seasonal variations. See Supplement S5 for configuration details and possibilities.

2.3.2 Aggregation of irrigated and rainfed vegetation

In contrast to previous versions of ISBA (Voirin-Morel, 2003; Calvet et al., 2008), there is no specific irrigated nature type in the new ECOCLIMAP-SG vegetation description. On the other hand, irrigation of all nature types is possible. The new irrigation scheme is able to represent the sub-grid heterogeneity of the irrigation fractional coverage. For each nature type, an irrigated and a non-irrigated fraction are considered at the simulation resolution. In order to prevent an excessive increase in the number of simulated nature types (potentially 20 non-irrigated and 20 irrigated times 3 irrigation types, i.e. a total of 120 types), involving a large increase of complexity, memory and computing cost, some choices were made for the implementation:

1. Selection of a limited number of irrigated nature types. The default implementation consists in six irrigated nature types. Temperate deciduous and evergreen trees types (No 8 and 10 in Table S1.2, respectively) can be used to represent fruits trees or olive trees for example, respectively. Shrub type (No 15) can be used to represent, among others, vine plants, and types No 19, 20 and 21 may represent irrigated crops (e.g. wheat, soybean, and corn, respectively).



2. Selection of the main irrigation method used for each grid cell and nature type, considering that in one grid cell there is only one dominant method for a given nature type (e.g. flooded rice in China or sprinkled corn in France).

Finally, the system state variables (soil water content, surface and soil temperature, vegetation biomass, etc.) differ in irrigated and non-irrigated parts of the cell. This implies to (1) duplicate a nature type if it is partially irrigated, (2) attribute for each grid cell the corresponding irrigated fraction, and (3) select the irrigation type for the irrigated fraction. Lastly, the two irrigated and non-irrigated nature types are treated separately but the same rooting depth and secondary parameters (see Table S1.1) are used.

In order to limit the computing time, vegetation types can (optionally) be gathered. In this case vegetation “patches” are created. In ISBA, patch aggregation (Masson et al., 2013) is a method used to reduce the number of simulated nature types. It is based on the aggregation of the fractions of nature types, as shown in Fig. 2. The model primary parameters such as rooting depth, LAI and tree height are weighted using the fractional coverage of each nature type in the grid cell. The mean parameter values are calculated following different laws: dominant, arithmetic averaging, inverse averaging or inverse of square logarithm averaging, depending on the considered parameters, as described in Noilhan and Lacarrère (1995) and Noilhan et al. (1997). In practice, the nature types to be aggregated (see the list in Fig. S1.1) within a grid cell are first chosen. Then, during the simulation, the fractions of nature type composing each patch are added together (step 1 in Fig. 2) for each grid cell. The different primary parameters (trees height, LAI, ...) are weighted by patch following the respective vegetation fractions (step 2 in Fig. 2). For secondary parameters (e.g. photosynthesis parameters in this study) a minimum number of patches is needed in order to avoid combining incompatible vegetation types (e.g. C3 crops and C4 crops).

In a first step (step 0 in Fig. 2) the differentiation between irrigated and rainfed nature types is done by computing the irrigated (and rainfed) fraction for each nature type and for each grid cell. Arithmetic averaging is used to cross information from the nature type fractional coverage and from the global irrigation fraction map described in Section 2.1.1. The ECOCLIMAP-SG land cover



classification uses this additional data layer to compute the fraction of irrigated vegetation at the spatial resolution of the model simulations. Each nature type considered as irrigated (by default 6) is duplicated
290 (meaning that for each of them a new nature type is created with the same parameters). This ensures the distinction of irrigated and rainfed soil water budget types. Then, as before, the nature types are aggregated by patch and the primary parameter values are computed (step 1 and step 2 in Fig. 2, respectively).

This change of the code structure based on the aggregation tool is a way to (1) maintain the
295 continuity with previous versions of the code, (2) ensure flexibility for the number of irrigated nature types to be considered and (3) simulate distinct irrigated and rainfed fractions of a nature type.

2.4 Model implementation and evaluation

The objective of the model evaluation is to demonstrate that the model is able to reproduce irrigation and that the irrigation scheme improves vegetation modelling and the associated surface fluxes as
300 compared to observations. We chose to study an area where the use of irrigation is well documented: the Continental United States (CONUS defined here as 20-55°N, 130-60°W, Fig. 1). In particular, we focused on a region where the irrigation is prominent: the south of the state of Nebraska (100-97°W, 40.25-41.25°N, Fig. 1e).

The ISBA LSM simulations (non-coupled with the atmosphere) are forced by the ERA-5
305 reanalysis at a spatial resolution of $0.25^\circ \times 0.25^\circ$ (Section 2.1.2) over a 40-year period from 1979 to 2018. The initial values of the soil moisture and soil temperature profiles are derived from a 20-year spin-up simulation by repeating year 1979. To evaluate the impact of irrigation, these simulations are run using ECOCLIMAP-SG. All nature types are grouped into 15 patches including three irrigated ones: shrubs (orchards), C3 (typically wheat and rice) and C4 crops (corn). This study focuses on the
310 results of these last two nature types because there are hardly any irrigated orchards in Nebraska in the irrigation map described in Section 2.1.1. The dates of the irrigation season were chosen in accordance with the literature (USDA and NASS, 2010) from May (emergence) to September (harvest), with a random picking of the day within those specific months. Three types of simulations were performed (Table 3): “ISBA_ref” without any irrigation (the benchmark), “ISBA_pheno” with only crop



315 phenology attributes (emergence and harvest dates) and the complete “ISBA_pheno_irr” simulation with irrigation and crop phenology attributes. For the comparison (ISBA_ref vs. ISBA_pheno vs. ISBA_pheno_irr), we selected areas where the irrigation fractional coverage is larger than 50 % as determined from the irrigation map.

In order to assess the consistency of the simulated irrigation process with observations, the 320 simulated number of yearly irrigation events on irrigated areas in Nebraska was compared with the USGS irrigation water amount estimates (Table 1). Since the latter consisted of 5-yearly means, only values of the mean and standard deviation of the yearly irrigation number were compared. Irrigation water amount was converted to a number of irrigation events using the model default irrigation water amount of 30 mm per irrigation event. The comparison was made for the irrigated croplands (either C3 325 or C4 crops) as defined using the irrigation map (Section 2.1.1) within the studied irrigated area in Nebraska (Fig. 1e).

The reference ISBA_ref LAI simulations were compared with those from ISBA_pheno and ISBA_pheno_irr experiments, and with the $0.01^\circ \times 0.01^\circ$ LAI satellite observations over areas in Nebraska where the vegetation is considered as C3 or C4 irrigated crops by ECOCLIMAP-SG.

330 In order to compare the time series simulations with observations, the correlation coefficient (R) and the root-mean-square difference (RMSD) scores were used. For water and carbon fluxes, they were calculated using daily values.

3 Results

The comparison between the model without irrigation (ISBA_ref experiment) before and after the 335 changes in the code structure (section 2.3) did not permit the detection of any impact on the model outputs (not shown). The results presented below are thus focused on the impacts of the crop phenology and irrigation implementation on the simulated land surface variables over Nebraska. In addition to these results, illustrations of the response to irrigation of simulated key land surface variables (SWI, LAI, GPP, evapotranspiration, LST) are shown over southwestern France and over the Hampton area in



340 Nebraska in Supplements S2 and S3, respectively. In the case of Hampton, it can be noticed that the simulated irrigation mainly occurs in July and August (Fig. S3.1).

3.1 Irrigation: water use

In Fig. 3, the mean yearly number of irrigation events for C3 and C4 crops for the ISBA_pheno_irr experiment is compared to the values derived from the observations from the USGS. The simulated
345 irrigation numbers present a large interannual variability, with a minimum of 2 in 1993 and a maximum close to 13 in 2002. It must be noticed that 1993 was one of the wettest year recorded at the Lincoln weather station (<https://lincolnweather.unl.edu/records/annual.asp>, last access August 2021) and that year 2012 was characterized by a prolonged drought. The mean simulated value of the yearly irrigation water amount used for irrigation (271 ± 75 mm year⁻¹) is almost identical to the observed one (264 ± 65
350 mm year⁻¹), with a difference of only +2.7%. This difference is small, although the model does not take into account the availability of the water resource yet.

3.2 Irrigation: plant growth

Figure 4 illustrates the mean seasonal and interannual variability of LAI in the most densely irrigated part of Nebraska for areas with a fraction of irrigated crops larger than 50 % in Fig. 1e, from 1999 to
355 2018. Table 4 presents the peak LAI characteristics. In all ISBA LAI simulations, the start of the growing season corresponds to a gradual increase in LAI from the initial value of LAI = $0.30 \text{ m}^2 \text{ m}^{-2}$ imposed to the model in winter. The observed LAI presents a smaller minimum LAI value of $0.15 \text{ m}^2 \text{ m}^{-2}$, starts increasing in April and a value of $0.30 \text{ m}^2 \text{ m}^{-2}$ is reached at the end of April. Then, plant growth continues at about the same low rate till the end of May. The LAI growth rate increases in June
360 and LAI reaches a mean peak value of $4.9 (\pm 0.8) \text{ m}^2 \text{ m}^{-2}$ is observed on 31 July (Table 4). The observed LAI then sharply decreases to reach its minimum value at about the end of September.

The ISBA_ref LAI simulations do not mirror the observed late growing season and rapid senescence. The ISBA_ref vs. observations comparison shows that without irrigation the simulated LAI generally starts increasing in March. On average, a peak LAI value of $3.6 (\pm 0.2) \text{ m}^2 \text{ m}^{-2}$ is simulated by
365 ISBA_ref on 2 July, before slowly decreasing until the end of December. The ISBA_ref growing season



is much longer than observed. It starts two months before the observations and stops three months after the observations. The simulated LAI peaks one month before the observations. The simulated yearly LAI amplitude is 28 % smaller than observed.

The ISBA_pheno LAI simulation is much more consistent with the LAI observations. The
370 growing season starts in mid-May and the senescence ends at the end of September. However, the simulated peak LAI is still 30 % smaller than observed ($\text{LAI} = 3.5 (\pm 0.2) \text{ m}^2 \text{ m}^{-2}$). The peak LAI is reached on 26 August, much later than the ISBA_ref peak LAI, and about one month after the observed peak. The sharp decrease of LAI in September results from harvests at random dates in September. Adding irrigation (ISBA_pheno_irr) does not change the general pattern of the LAI curve, but increases
375 the LAI amplitude, with a mean peak LAI value of $3.7 (\pm 0.1) \text{ m}^2 \text{ m}^{-2}$ on 28 August, larger (+8%) than for ISBA_pheno but still below the observation (-24%).

The interannual variability of simulated and observed LAI values is illustrated in Fig. 4b, from 2002 to 2008. The ISBA_ref LAI presents a systematic drop in summer, which is not present in the observations nor simulated by the ISBA_pheno and ISBA_pheno_irr experiments. Without the regular
380 seasonality imposed by crop phenology parameters, the model may simulate a re-growth of vegetation in autumn (e.g. in 2003), that is not present in the observations. The ISBA_pheno and ISBA_pheno_irr simulations are more consistent with the observed seasonality.

3.3 Impact of crop phenology and irrigation on LAI at a regional scale

This section is focused on the impact of irrigation practices for the south Nebraska zone (as defined in
385 Fig. 1e), and all nature types are considered for the comparison with observations at a spatial resolution of $0.25^\circ \times 0.25^\circ$.

Figure 5a shows the seasonal mean LAI variations from 1999 to 2018. This Figure is similar to Fig. 4a but all nature types are considered. Peak LAI characteristics are given in Table 4. They differ from the crop LAI peaks. While, the observed LAI peaks at $3.8 (\pm 1.5) \text{ m}^2 \text{ m}^{-2}$ on 31 July for ISBA_ref, LAI peaks at $3.3 (\pm 0.3) \text{ m}^2 \text{ m}^{-2}$ on 1 July for ISBA_ref, $3.1 (\pm 0.3) \text{ m}^2 \text{ m}^{-2}$ on 16 July for ISBA_pheno,
390 and $3.1 (\pm 0.3) \text{ m}^2 \text{ m}^{-2}$ on 16 July for ISBA_pheno_irr. Compared to crop simulations, the experiments with crop phenology (ISBA_pheno and ISBA_pheno_irr) present earlier peak LAI dates, due to the



impact of rainfed vegetation. However, the irrigated crop signature is visible in the second peak of the annual LAI cycle simulated by ISBA_pheno and ISBA_pheno_irr experiments at the end of August. More often than not (83 % and 88 % of the grid cells for R and RMSD, respectively) the LAI score differences between ISBA_pheno_irr and ISBA_ref shown in Fig. 5 correspond to an improvement of the LAI simulation with the representation of irrigation. A month by month analysis of the scores (Fig. 6) shows a marked improvement of R values in June, July and September. The R value can frequently be increased by 30%. Lower RMSD values are observed from April to November, more frequently in May and in October. In April, October and November, the main cause of the reduction in RMSD values is the imposed minimum value of $0.3 \text{ m}^2 \text{ m}^{-2}$ before the emergence (in May) and the harvest (in September).

3.4 Impact on the GPP flux

As the vegetation productivity is linked to LAI, the seasonality pattern of GPP (Fig. 7) is comparable to the one of LAI (Fig. 5) but the observed GPP peak ($9.2 \pm 2.1 \text{ g[C].m}^{-2}.\text{day}^{-1}$) occurs on mid-July while the observed LAI peaks on 31 July. During the plant growing period, the smallest differences between all the simulations and the observations occur at about the same time as the observed GPP peak. For all simulations, a GPP plateau at a value of $9.0 \pm 1.8 \text{ g[C] m}^{-2} \text{ day}^{-1}$ is reached at the beginning of July and lasts until mid-July. Finally the simulated GPP decreases in September with a delay of about two weeks with respect to the observations.

Before July, the ISBA_ref photosynthetic activity is well in advance as compared to the observations, of about 20 days in May. This is consistent with the very large LAI values simulated by ISBA_ref in May: about $2 \text{ m}^2 \text{ m}^{-2}$, while the mean LAI observation hardly exceeds $0.5 \text{ m}^2 \text{ m}^{-2}$. The simulated GPP maximum ($9.7 \pm 2.0 \text{ g[C] m}^{-2} \text{ day}^{-1}$) is reached before the end of June. After a sharp decrease at the end of June, the ISBA_ref GPP decreases at a slower rate than the observations. From mid-September to the end of October, the simulated GPP is much larger than the observed GPP.

The ISBA_ref flaws are much less pronounced in ISBA_pheno and ISBA_pheno_irr experiments. In the latter simulations, the increase of the GPP occurs at about the same time as in the observations. The GPP values are systematically larger with irrigation in July and August than for other



420 simulations. As for LAI, the GPP R and RMSD scores (Fig. 7b and 7c, respectively) are better for ISBA_pheno_irr than for ISBA_ref, with an improvement on 87 % and 81 % over the domain, respectively.

3.5 Impact on evapotranspiration

Investigating evapotranspiration is a way to assess the impact of irrigation on the hydrological system. Figure 8 shows evapotranspiration for the ISBA simulations and for GLEAM. This Figure is similar to Figs. 5 and 7 but a shorter time period is considered, from 2003 to 2018. Before the irrigation period, the observed evapotranspiration steadily increases from February to July. After the irrigation period, evapotranspiration decreases until November. It can be observed that the short term variability of the GLEAM evapotranspiration is represented well by the simulations. On the other hand, all ISBA simulations produce much larger evapotranspiration values than GLEAM during the growing period from April to June. For example, all ISBA simulations can reach 5 mm day^{-1} while GLEAM does not exceed 3.5 mm day^{-1} . Over this time period, ISBA_ref overestimates evapotranspiration with respect to GLEAM by $0.98 \pm 0.42 \text{ mm day}^{-1}$ ($38 \pm 16 \%$) on average.

On the contrary, from mid-July to mid-August, all ISBA simulations tend to underestimate evapotranspiration with respect to GLEAM, by up to 1.3 mm day^{-1} for ISBA_ref. Accounting for crop phenology and irrigation into the model has a substantial impact on this variable and reduces the bias. Over the whole irrigation period, the mean bias goes from $-0.4 \pm 0.4 \text{ mm day}^{-1}$ ($-13 \pm 12 \%$) for ISBA_ref to $-0.2 \pm 0.3 \text{ mm day}^{-1}$ ($-7 \pm 11 \%$) and $-0.1 \pm 0.3 \text{ mm day}^{-1}$ ($-2 \pm 11 \%$) for ISBA_pheno and ISBA_pheno_irr, respectively. Evapotranspiration is overestimated again after the harvest, from mid-September to November by $0.38 \pm 0.18 \text{ mm day}^{-1}$ ($42 \pm 20 \%$ compared to the observations).

The newly implemented processes have a small but positive impact on the bias before and after the irrigation period. During the growing season, from April to June, the overestimation decreases from 38 % in ISBA_ref to 33 % and 34 % for ISBA_pheno and ISBA_pheno_irr, respectively. From mid-September to November, the overestimation decreases from 42 % to 35 % and 36 %, respectively. The R and RMSD differences between ISBA_ref and ISBA_pheno_irr (Fig. 8) also show a global improvement with 83 % and 79 % of the grid cells being improved. However, the effect on the R score



is small (less than 0.1) and heterogeneous in time and space. Figure 9 shows that the R score is mainly improved in August and in September, before the harvest. The improvement of RMSD is more stable, and can be observed from May to October, the impact being more pronounced in July and August.

450 3.6 Impact on LST

In order to evaluate the impact of irrigation on the land surface energy budget, Figure 10 shows land surface temperature at 12h00 local time simulated by the three model configurations and derived from the CGLS product. Overall, ISBA tends to overestimate LST at noon, especially in April-May, up to 7 °C in Fig. 10a. The bias is reduced during the summer.

455 Due to the difficulty of observing the differences between the simulations, Figure 10b presents differences of ISBA_pheno and ISBA_pheno_irr versus ISBA_ref. With crop phenology (with or without irrigation) the simulated LST is globally higher from April to June and from mid-September to November. The maximum difference with respect to ISBA_ref is $+0.7 \pm 0.3$ °C. It is observed for ISBA_pheno in September. During the summer (July and August) the new model versions tend to
460 present lower LST values, with temperature differences close to -0.2 ± 0.1 °C in ISBA_pheno_irr. Moreover, from May to mid-September the temperature in ISBA_pheno_irr is lower than in ISBA_pheno, and this difference can reach locally -0.9 °C in summer. Figure 11 presents the monthly R and RMSD scores of ISBA_ref with respect to CGLS LST observations and the ISBA_pheno_irr score difference is shown. It shows that there is a seasonal dependence of these statistical values, with slightly
465 better R and RMSD scores observed for ISBA_pheno_irr in July and August during the irrigation period. However, the representation of irrigation tends to degrade RMSD before (April, May) and after (October, November) the irrigation period.

4 Discussion and perspectives

The results presented in Section 3 show that the new version of ISBA is able to produce a realistic
470 yearly irrigation water amount (Fig. 3). It also markedly improves the LAI and GPP simulations (Fig. 4-5 and Fig. 7, respectively). On the other hand, the new ISBA version developed in this study has a



limited impact on the evapotranspiration and on the LST simulations and is not able to significantly reduce the strong model biases that are observed for these variables before and after the irrigation time period (Fig. 8-10).

475 **4.1 Could the new irrigation scheme be further improved?**

The results of our numerical experiments over Nebraska show that considering crop phenology and irrigation improves the consistency of the simulations with LAI and GPP observations. The corresponding correlation and RMSD scores are improved. Two new developments can explain this behaviour: (1) the crop phenology parameters used to force emergence and harvest dates reduce the
480 length of the growing season, delay spring growth and avoid a regrowth in the autumn, and (2) the irrigation limits the water stress and enhances plant growth at summertime. Nevertheless they both have shortcomings and their performance could be limited by difficulties in simulating processes that are not directly related to irrigation.

Firstly, the same emergence and harvest dates are imposed for all years, while in reality crop
485 phenology may present an inter-annual variability related to climate conditions. This is particularly the case for Nebraska because the start of the growing season depends on the snow melt and soil thawing dates. These processes are represented in ISBA and crop phenology parameters could be related to snow melting and soil thawing, but this would require extensive developments to be implemented at a global scale. Moreover, the representation of the cold season processes is not perfect in ISBA (Decharme et al.
490 2019) and this could explain biases in soil temperature and LST simulations before and after the irrigation time period. Figure 10 shows that LST values below the freezing level can be observed in April and that their model counterparts are about 7 °C warmer. The earlier thawing in model simulations is reflected in the much earlier leaf onset in LAI simulations. Figure 5 shows that while the observed LAI does not exceed 0.5 m² m⁻² at the end of April, the ISBA_ref LAI reaches the same value
495 about one month earlier. The unrealistically early leaf onset is consistent with the warm model bias at the end of the cold season. This shows that improving the representation of the cold season by assimilating satellite-derived or in situ snow cover fraction observations could improve the simulation



of the crop growing period in this area. However, the currently used empirical approach to establish the crop season provides robust results over the irrigated grid cells (Fig. 4).

500 Secondly, the irrigation itself is based on fixed parameter values such as the minimum period between two consecutive irrigations (one week) and SWI levels triggering irrigation turns. The simulations over the Hampton grid cell show that the first irrigation can start at quite low levels of the SWI (Fig. S3.1), even below the second irrigation threshold of 0.55 defined in Section 2.3.1. Suppressing the one week constraint of irrigation turns improves the simulation of the peak LAI, which
505 otherwise is rather poorly simulated (Fig. 4). However, this change triggers unrealistic large irrigation water amounts (not shown). A lack of irrigation water amount cannot explain the excessive soil water deficit. One could also challenge the quality of the ERA5 precipitation. Figure S4.1 and Fig. S4.2 show that ERA5 precipitation compares well with in situ observations and that the seasonal and inter-annual variability is fairly represented. A more plausible explanation could be that the initial soil water storage
510 value between the end of the cold season and the first irrigation turn is withdrawn too quickly from the soil by the model. This explanation would be consistent with the marked overestimation of evapotranspiration in spring, from April to June (Fig. 8), before the irrigation time period.

In order to investigate the evapotranspiration bias in spring, the evaporation components were plotted in Fig. S3.3 and Fig. S3.4 for the Hampton irrigated area in 2018. Figure S3.3 shows that total
515 evapotranspiration of ISBA_ref and ISBA_pheno_irr are quite similar. This is consistent with the small impact of crop phenology on total evapotranspiration showed in Fig. 8. On the other hand, soil evaporation and plant transpiration differ. In the ISBA_pheno_irr simulation, transpiration is reduced in spring by 30 % to more than 100 %, in comparison with ISBA_ref. The lower transpiration is compensated by larger soil evaporation values. As a result, total evapotranspiration does not change
520 much and the bias is not reduced in ISBA_pheno_irr. Also, Fig. S3.4 shows that the new irrigation module does not affect interception much. Therefore, the ISBA_pheno_irr evapotranspiration bias in spring could be caused by the large soil evaporation. The evaporation component could be overestimated because (1) the soil is too warm in relation to a poor representation of thawing or because (2) crop residues at the soil surface are not represented. Wortmann et al. (2012) showed that in this area,



525 not harvesting crop residues tends to reduce soil evaporation and increase crop yield, limit water runoff,
soil erosion, and contributes to maintaining soil fertility. The ISBA model includes a representation of
litter in forests (Napoly et al. 2017) that will be generalized to low vegetation in the next version of
SURFEX. Using this new capability could improve our simulations.

4.2 Is the irrigation scheme flexible enough?

530 In this study, sprinkling irrigation was considered. The model is able to represent other irrigation
systems such as flooding irrigation but more developments are needed to limit the runoff to the irrigated
plot and this options needs to be validated. The newly implemented irrigation processes, along with the
new ECOCLIMAP-SG vegetation description let users choose which nature type should be irrigated.
Irrigation can be represented at various spatial scales, ranging from the field scale for agricultural
535 studies to the global scale for climate studies. Model parameters can be specified using new datasets or
local characteristics. For example, in this article we used a unique date for starting and ending the crop
growing season with a random variability, but more accurate dates could be prescribed (varying
spatially and from one vegetation type to another, or using crop calendars). Moreover, the better spatial
resolution of ECOCLIMAP-SG allows the use of high resolution atmospheric forcing. This provides
540 new opportunities for assessing the impact of irrigation on local climate and water resource conditions.

This study is mainly focused on a zone in the south of Nebraska where the irrigation density is
relatively high (Fig 3), and results could differ in other regions. Except for the fixed emergence and
harvesting dates corresponding to regional crop phenology (from USDA and NASS, 2010), default
values are used for all the other parameters (Section 2.4). Tests performed in southwestern France
545 (Supplement S2) allowed ensuring that the model is able to work in contrasting climate conditions.

In this study, the ISBA simulations were not coupled to the atmosphere, nor to the CTRIP river
routing system. Such coupled numerical experiments could be performed thanks to the SURFEX
modelling platform. However, more developments are needed in order to ensure water conservation in
the hydrological system. In particular, irrigation water amounts should be consistent with the available
550 water resource in rivers, groundwater, and dams.



5 Conclusions

A new uncalibrated irrigation scheme was implemented within the ISBA land surface model in order to improve the representation of vegetation over agricultural areas. A case study over an irrigated area in the state of Nebraska (USA) was performed to validate the new scheme. Simple crop phenology rules represent emergence and harvesting and improve the seasonality of plant growth, while the additional water supply from the irrigation mostly impacts the peak LAI value. The model is able to produce a realistic yearly irrigation water amount and markedly improves the LAI and GPP. It is shown that model performance can be limited by processes not directly related to irrigation, such as thawing or crop residues. The irrigation scheme has many possible configurations and the code is highly flexible. With this capability, ancillary data on farming practices such as emergence and harvest dates, or the amount of water per irrigation event, could be used.

Code availability

The ISBA land surface model is available as open source via the SURFEX modelling platform, available at <https://www.umr-cnrm.fr/surfex/spip.php?article387>. It is under a CECILL-C License (French equivalent to the L-GPL licence). The version developed and use for the experiment in this study is available in the git-hub: https://github.com/ArseneD/OPEN_SURFEX_V81_IRR. It based on the SURFEX version 8.1 (ref f70f6457). For future use, it is strongly recommended to use the newest version of ISBA, from the version 9.0 (scheduled for release in 2020) from which the irrigation developed will be included by default.

Author contribution

Arsène Druel and Clément Albergel designed the experiments. Arsène Druel carried out the implementation of the irrigation scheme and performed the simulations. Arsène Druel wrote the



575 manuscript. All co-authors participated to the analysis of the results and to the revision of the
manuscript.

Competing interests

The authors declare that they have no conflicts of interest.

Acknowledgments

580 The work presented here was supported by the project URCLIM (advance on URban CLIMate services,
part of ERA4CS, an ERA-NET initialised by JPI Climate with co-funding of the European Union
(Grant n°690462)). The authors would like to thanks Stephanie Faroux and Marie Minvielle in charge
of the SURFEX code support for technical assistance, and Deborah Verfaillie for her careful reading of
the manuscript.



585 References

- Adegoke, J. O., Pielke, R. A., Eastman, J., Mahmood, R. and Hubbard, K. G.: Impact of Irrigation on Midsummer Surface Fluxes and Temperature under Dry Synoptic Conditions: A Regional Atmospheric Model Study of the U.S. High Plains, *Mon. Weather Rev.*, 131(3), 556–564, [https://doi.org/10.1175/1520-0493\(2003\)131<0556:IOIOMS>2.0.CO;2](https://doi.org/10.1175/1520-0493(2003)131<0556:IOIOMS>2.0.CO;2), 2003.
- 590 AQUASTAT and FAO: Country Fact Sheet, United States of America, [online] Available from: http://www.fao.org/nr/water/aquastat/data/cf/readPdf.html?f=USA-CF_eng.pdf (Accessed 20 March 2019), 2019.
- Baret, F., Weiss, M., Lacaze, R., Camacho, F., Makhmara, H., Pacholczyk, P. and Smets, B.: GEOV1: LAI and FAPAR essential climate variables and FCOVER global time series capitalizing over
595 existing products. Part1: Principles of development and production, *Remote Sens. Environ.*, 137, 299–309, <https://doi.org/10.1016/j.rse.2012.12.027>, 2013.
- Beck, H. E., Pan, M., Roy, T., Weedon, G. P., Pappenberger, F., van Dijk, A. I. J. M., Huffman, G. J., Adler, R. F., and Wood, E. F.: Daily evaluation of 26 precipitation datasets using Stage-IV gauge-radar data for the CONUS, *Hydrol. Earth Syst. Sci.*, 23, 207–224, [https://doi.org/10.5194/hess-23-](https://doi.org/10.5194/hess-23-207-2019)
600 207-2019, 2019.
- Biemans, H., Haddeland, I., Kabat, P., Ludwig, F., Hutjes, R. W. A., Heinke, J., von Bloh, W. and Gerten, D.: Impact of reservoirs on river discharge and irrigation water supply during the 20th century, *Water Resour. Res.*, 47(3), <https://doi.org/10.1029/2009WR008929>, 2011.
- Broadbent, A. M., Coutts, A. M., Tapper, N. J. and Demuzere, M.: The cooling effect of irrigation on
605 urban microclimate during heatwave conditions, *Urban Clim.*, 23, 309–329, <https://doi.org/10.1016/j.uclim.2017.05.002>, 2018.
- Brown, T. C., Foti, R. and Ramirez, J. A.: Projected freshwater withdrawals in the United States under a changing climate, *Water Resour. Res.*, 49(3), 1259–1276, <https://doi.org/10.1002/wrcr.20076>, 2013.
- Bruinsma, J.: The Resource Outlook to 2050: By How Much Do Land, Water Use and Crop Yields
610 Need to Increase by 2050?, Food and Agriculture Organization, Rome, Italy., 2009.
- Calvet, J.-C., and Champeaux J.-L.: L’apport de la télédétection spatiale à la modélisation des surfaces



- continentales. *La Météorologie*, 108, 52–58, <https://doi.org/10.37053/lameteorologie-2020-0016>, 2020.
- 615 Calvet, J.-C., Gibelin, A.-L., Roujean, J.-L., Martin, E., Le Moigne, P., Douville, H. and Noilhan, J.:
Past and future scenarios of the effect of carbon dioxide on plant growth and transpiration for three
vegetation types of southwestern France, *Atmospheric Chem. Phys.*, 8(2), 397–406,
<https://doi.org/10.5194/acp-8-397-2008>, 2008.
- 620 Calvet, J.-C., Noilhan, J., Roujean, J.-L., Bessemoulin, P., Cabelguenne, M., Olioso, A. and Wigneron,
J.-P.: An interactive vegetation SVAT model tested against data from six contrasting sites, *Agric.
For. Meteorol.*, 92(2), 73–95, [https://doi.org/10.1016/S0168-1923\(98\)00091-4](https://doi.org/10.1016/S0168-1923(98)00091-4), 1998.
- Carrillo-Guerrero, Y., Glenn, E. P. and Hinojosa-Huerta, O.: Water budget for agricultural and aquatic
ecosystems in the delta of the Colorado River, Mexico: Implications for obtaining water for the
environment, *Ecol. Eng.*, 59, 41–51, <https://doi.org/10.1016/j.ecoleng.2013.04.047>, 2013.
- 625 Chukalla, A. D., Krol, M. S. and Hoekstra, A. Y.: Green and blue water footprint reduction in irrigated
agriculture: effect of irrigation techniques, irrigation strategies and mulching, *Hydrol. Earth Syst.
Sci.*, 19(12), 4877–4891, <https://doi.org/10.5194/hess-19-4877-2015>, 2015.
- Colaizzi, P. D., Gowda, P. H., Marek, T. H. and Porter, D. O.: Irrigation in the Texas High Plains: a
brief history and potential reductions in demand, *Irrig. Drain.*, 58(3), 257–274,
<https://doi.org/10.1002/ird.418>, 2009.
- 630 DeAngelis, A., Dominguez, F., Fan, Y., Robock, A., Kustu, M. D. and Robinson, D.: Evidence of
enhanced precipitation due to irrigation over the Great Plains of the United States, *J. Geophys. Res.*,
115(D15), D15115, <https://doi.org/10.1029/2010JD013892>, 2010.
- 635 Decharme, B., Delire, C., Minvielle, M., Colin, J., Vergnes, J., Alias, A., Saint-Martin, D., Séférian, R.,
Sénési, S. and Voldoire, A.: Recent Changes in the ISBA-CTRIP Land Surface System for Use in the
CNRM-CM6 Climate Model and in Global Off-Line Hydrological Applications, *J. Adv. Model.
Earth Syst.*, 11(5), 1207–1252, <https://doi.org/10.1029/2018MS001545>, 2019.
- Döll, P., Fiedler, K. and Zhang, J.: Global-scale analysis of river flow alterations due to water
withdrawals and reservoirs, *Hydrol. Earth Syst. Sci.*, 13(12), 2413–2432,



- <https://doi.org/10.5194/hess-13-2413-2009>, 2009.
- 640 Döll, P., Hoffmann-Dobrev, H., Portmann, F. T., Siebert, S., Eicker, A., Rodell, M., Strassberg, G. and Scanlon, B. R.: Impact of water withdrawals from groundwater and surface water on continental water storage variations, *J. Geodyn.*, 59–60, 143–156, <https://doi.org/10.1016/j.jog.2011.05.001>, 2012.
- Douglas, E. M., Niyogi, D., Frolking, S., Yeluripati, J. B., Pielke, R. A., Niyogi, N., Vörösmarty, C. J. and Mohanty, U. C.: Changes in moisture and energy fluxes due to agricultural land use and irrigation in the Indian Monsoon Belt, *Geophys. Res. Lett.*, 33(14), L14403, <https://doi.org/10.1029/2006GL026550>, 2006.
- 645
- Evans, R. G. and Sadler, E. J.: Methods and technologies to improve efficiency of water use, *Water Resour. Res.*, 44(7), <https://doi.org/10.1029/2007WR006200>, 2008.
- 650
- FAO: Food and Agriculture Organization of the United Nations: Water withdrawal and pressure on water resources, [online] Available from: <http://www.fao.org/nr/water/aquastat/didyouknow/index2.stm>, http://www.fao.org/nr/water/aquastat/infographics/Withdrawal_eng.pdf (Accessed 9 October 2019), 2014.
- 655
- Faroux, S., Kaptué Tchuenté, A. T., Roujean, J.-L., Masson, V., Martin, E. and Le Moigne, P.: ECOCLIMAP-II/Europe: a twofold database of ecosystems and surface parameters at 1 km resolution based on satellite information for use in land surface, meteorological and climate models, *Geosci. Model Dev.*, 6(2), 563–582, <https://doi.org/10.5194/gmd-6-563-2013>, 2013.
- Field, C. B., Barros, V. R., Dokken, D. J., Mach, K. J. and Mastrandrea, M. D., Eds.: *Climate Change 2014 Impacts, Adaptation, and Vulnerability: Working Group II Contribution to the Fifth Assessment Report of the Intergovernmental Panel on Climate Change*, Cambridge University Press, Cambridge., 2014.
- 660
- Fischer, C., Montmerle, T., Berre, L., Auger, L. and Ștefănescu, S. E.: An overview of the variational assimilation in the ALADIN/France numerical weather-prediction system, *Q. J. R. Meteorol. Soc.*, 131(613), 3477–3492, <https://doi.org/10.1256/qj.05.115>, 2005.
- 665



- Fraiture, C. de, Wichelns, D., Rockström, J., Kemp-Benedict, E., Eriyagama, N., Gordon, L. J., Hanjra, M. A., Hoogeveen, J., Huber-Lee, A. and Karlberg, L.: Looking ahead to 2050: scenarios of alternative investment approaches, in In Molden, David (Ed.). *Water for food, water for life: a Comprehensive Assessment of Water Management in Agriculture.*, pp. 91–145, International Water Management Institute (IWMI), London, UK: Earthscan; Colombo, Sri Lanka. [online] Available from: <https://hdl.handle.net/10568/36869>, 2007.
- Freitas, S. C., Trigo, I. F., Macedo, J., Barroso, C., Silva, R. and Perdigão, R.: Land surface temperature from multiple geostationary satellites, *Int. J. Remote Sens.*, 34(9–10), 3051–3068, <https://doi.org/10.1080/01431161.2012.716925>, 2013.
- Gibelin, A.-L., Calvet, J.-C., Roujean, J.-L., Jarlan, L. and Los, S. O.: Ability of the land surface model ISBA-A-gs to simulate leaf area index at the global scale: Comparison with satellites products, *J. Geophys. Res.*, 111(D18), D18102, <https://doi.org/10.1029/2005JD006691>, 2006.
- Grafton, R. Q., Williams, J., Perry, C. J., Molle, F., Ringler, C., Steduto, P., Udall, B., Wheeler, S. A., Wang, Y., Garrick, D. and Allen, R. G.: The paradox of irrigation efficiency, *Science*, 361(6404), 748–750, <https://doi.org/10.1126/science.aat9314>, 2018.
- Haddeland, I., Skaugen, T. and Lettenmaier, D. P.: Anthropogenic impacts on continental surface water fluxes, *Geophys. Res. Lett.*, 33(8), L08406, <https://doi.org/10.1029/2006GL026047>, 2006.
- Hanasaki, N., Inuzuka, T., Kanae, S. and Oki, T.: An estimation of global virtual water flow and sources of water withdrawal for major crops and livestock products using a global hydrological model, *J. Hydrol.*, 384(3–4), 232–244, <https://doi.org/10.1016/j.jhydrol.2009.09.028>, 2010.
- Harding, R. J., Blyth, E. M., Tuinenburg, O. A. and Wiltshire, A.: Land atmosphere feedbacks and their role in the water resources of the Ganges basin, *Sci. Total Environ.*, 468–469, S85–S92, <https://doi.org/10.1016/j.scitotenv.2013.03.016>, 2013.
- Hersbach, H. and Dee, D.: ERA5 reanalysis is in production, *ECMWF Newsl.* No 147, 7, 2016.
- Hoekstra, A. Y. and Mekonnen, M. M.: The water footprint of humanity, *Proc. Natl. Acad. Sci.*, 109(9), 3232–3237, <https://doi.org/10.1073/pnas.1109936109>, 2012.
- Jiang, L., Ma, E. and Deng, X.: Impacts of Irrigation on the Heat Fluxes and Near-Surface Temperature



- in an Inland Irrigation Area of Northern China, *Energies*, 7(3), 1300–1317, <https://doi.org/10.3390/en7031300>, 2014.
- 695 Jung, M., Reichstein, M., Schwalm, C. R., Huntingford, C., Sitch, S., Ahlström, A., Arneeth, A., Camps-Valls, G., Ciais, P., Friedlingstein, P., Gans, F., Ichii, K., Jain, A. K., Kato, E., Papale, D., Poulter, B., Raduly, B., Rödenbeck, C., Tramontana, G., Viovy, N., Wang, Y.-P., Weber, U., Zaehle, S. and Zeng, N.: Compensatory water effects link yearly global land CO₂ sink changes to temperature, *Nature*, 541(7638), 516–520, <https://doi.org/10.1038/nature20780>, 2017.
- 700 Khan, S. and Abbas, A.: Upscaling water savings from farm to irrigation system level using GIS-based agro-hydrological modelling, *Irrig. Drain.*, 56(1), 29–42, <https://doi.org/10.1002/ird.284>, 2007.
- Koech, R. and Langat, P.: Improving Irrigation Water Use Efficiency: A Review of Advances, Challenges and Opportunities in the Australian Context, *Water*, 10(12), 1771, <https://doi.org/10.3390/w10121771>, 2018.
- 705 Kueppers, L. M., Snyder, M. A. and Sloan, L. C.: Irrigation cooling effect: Regional climate forcing by land-use change, *Geophys. Res. Lett.*, 34(3), L03703, <https://doi.org/10.1029/2006GL028679>, 2007.
- Lawston, P. M., Santanello, J. A., Zaitchik, B. F. and Rodell, M.: Impact of Irrigation Methods on Land Surface Model Spinup and Initialization of WRF Forecasts, *J. Hydrometeorol.*, 16(3), 1135–1154, <https://doi.org/10.1175/JHM-D-14-0203.1>, 2015.
- 710 Le Moigne, P. et al.: SURFEX scientific documentation - V8.1, Sci. Doc. - SURFEX [online] Available from: <http://www.umr-cnrm.fr/surfex/spip.php?rubrique11> (Accessed 26 February 2018), 2018.
- Lobell, D. B., Bonfils, C. J., Kueppers, L. M. and Snyder, M. A.: Irrigation cooling effect on temperature and heat index extremes, *Geophys. Res. Lett.*, 35(9), L09705, <https://doi.org/10.1029/2008GL034145>, 2008.
- 715 Martens, B., Miralles, D. G., Lievens, H., van der Schalie, R., de Jeu, R. A. M., Fernández-Prieto, D., Beck, H. E., Dorigo, W. A. and Verhoest, N. E. C.: GLEAM v3: satellite-based land evaporation and root-zone soil moisture, *Geosci. Model Dev.*, 10(5), 1903–1925, <https://doi.org/10.5194/gmd-10-1903-2017>, 2017.
- Masson, V., Le Moigne, P., Martin, E., Faroux, S., Alias, A., Alkama, R., Belamari, S., Barbu, A.,



- 720 Boone, A., Bouyssel, F., Brousseau, P., Brun, E., Calvet, J.-C., Carrer, D., Decharme, B., Delire, C.,
Donier, S., Essaouini, K., Gibelin, A.-L., Giordani, H., Habets, F., Jidane, M., Kerdraon, G.,
Kourzeneva, E., Lafaysse, M., Lafont, S., Lebeaupin Brossier, C., Lemonsu, A., Mahfouf, J.-F.,
Marguinaud, P., Mokhtari, M., Morin, S., Pigeon, G., Salgado, R., Seity, Y., Taillefer, F., Tanguy,
G., Tulet, P., Vincendon, B., Vionnet, V. and Voltaire, A.: The SURFEXv7.2 land and ocean
725 surface platform for coupled or offline simulation of earth surface variables and fluxes, *Geosci.
Model Dev.*, 6(4), 929–960, <https://doi.org/10.5194/gmd-6-929-2013>, 2013.
- Meier, J., Zabel, F. and Mauser, W.: A global approach to estimate irrigated areas – a
comparison between different data and statistics, *Hydrol. Earth Syst. Sci.*, 22(2), 1119–1133,
<https://doi.org/10.5194/hess-22-1119-2018>, 2018.
- 730 Noilhan, J. and Lacarrère, P.: GCM Grid-Scale Evaporation from Mesoscale Modeling, *J. Clim.*, 8(2),
206–223, [https://doi.org/10.1175/1520-0442\(1995\)008<0206:GGSEFM>2.0.CO;2](https://doi.org/10.1175/1520-0442(1995)008<0206:GGSEFM>2.0.CO;2), 1995.
- Noilhan, J. and Planton, S.: A Simple Parameterization of Land Surface Processes for Meteorological
Models, *Mon. Weather Rev.*, 117(3), 536–549, [https://doi.org/10.1175/1520-0493\(1989\)117<0536:ASPOLS>2.0.CO;2](https://doi.org/10.1175/1520-0493(1989)117<0536:ASPOLS>2.0.CO;2), 1989.
- 735 Noilhan, J., Lacarrère, P., Dolman, A. J. and Blyth, E. M.: Defining area-average parameters in
meteorological models for land surfaces with mesoscale heterogeneity, *J. Hydrol.*, 190(3–4), 302–
316, [https://doi.org/10.1016/S0022-1694\(96\)03131-9](https://doi.org/10.1016/S0022-1694(96)03131-9), 1997.
- Ozdogan, M., Rodell, M., Beaudoin, H. K. and Toll, D. L.: Simulating the Effects of Irrigation over
the United States in a Land Surface Model Based on Satellite-Derived Agricultural Data, *J.*
740 *Hydrometeorol.*, 11(1), 171–184, <https://doi.org/10.1175/2009JHM1116.1>, 2010.
- Perry, C., Steduto, P. and Karejeh, F.: Does Improved Irrigation Technology Save Water? A Review of
the Evidence, Food and Agriculture Organization, Cairo, Egypt., 2017.
- Pfeiffer, L. and Lin, C.-Y. C.: Does efficient irrigation technology lead to reduced groundwater
extraction? Empirical evidence, *J. Environ. Econ. Manag.*, 67(2), 189–208,
745 <https://doi.org/10.1016/j.jeem.2013.12.002>, 2014.
- Piao, S., Ciais, P., Huang, Y., Shen, Z., Peng, S., Li, J., Zhou, L., Liu, H., Ma, Y., Ding, Y.,



- Friedlingstein, P., Liu, C., Tan, K., Yu, Y., Zhang, T. and Fang, J.: The impacts of climate change on water resources and agriculture in China, *Nature*, 467(7311), 43–51, <https://doi.org/10.1038/nature09364>, 2010.
- 750 Puma, M. J. and Cook, B. I.: Effects of irrigation on global climate during the 20th century, *J. Geophys. Res.*, 115(D16), D16120, <https://doi.org/10.1029/2010JD014122>, 2010.
- Rodell, M., Velicogna, I. and Famiglietti, J. S.: Satellite-based estimates of groundwater depletion in India, *Nature*, 460(7258), 999–1002, <https://doi.org/10.1038/nature08238>, 2009.
- Rost, S., Gerten, D., Bondeau, A., Lucht, W., Rohwer, J. and Schaphoff, S.: Agricultural green and blue
755 water consumption and its influence on the global water system: GLOBAL WATER USE IN AGRICULTURE, *Water Resour. Res.*, 44(9), <https://doi.org/10.1029/2007WR006331>, 2008.
- Sacks, W. J., Cook, B. I., Buening, N., Levis, S. and Helkowski, J. H.: Effects of global irrigation on the near-surface climate, *Clim. Dyn.*, 33(2–3), 159–175, <https://doi.org/10.1007/s00382-008-0445-z>, 2009.
- 760 Saeed, F., Hagemann, S. and Jacob, D.: Impact of irrigation on the South Asian summer monsoon, *Geophys. Res. Lett.*, 36(20), L20711, <https://doi.org/10.1029/2009GL040625>, 2009.
- Shukla, S. P., Puma, M. J. and Cook, B. I.: The response of the South Asian Summer Monsoon circulation to intensified irrigation in global climate model simulations, *Clim. Dyn.*, 42(1–2), 21–36, <https://doi.org/10.1007/s00382-013-1786-9>, 2014.
- 765 Siebert, S. and Döll, P.: Quantifying blue and green virtual water contents in global crop production as well as potential production losses without irrigation, *J. Hydrol.*, 384(3–4), 198–217, <https://doi.org/10.1016/j.jhydrol.2009.07.031>, 2010.
- Siebert, S., Kumm, M., Porkka, M., Döll, P., Ramankutty, N. and Scanlon, B. R.: A global data set of the extent of irrigated land from 1900 to 2005, *Hydrol. Earth Syst. Sci.*, 19(3), 1521–1545,
770 <https://doi.org/10.5194/hess-19-1521-2015>, 2015.
- Sorooshian, S., Li, J., Hsu, K. and Gao, X.: Influence of irrigation schemes used in regional climate models on evapotranspiration estimation: Results and comparative studies from California’s Central Valley agricultural regions: INFLUENCE OF IRRIGATION IN RCM ON ET, *J. Geophys. Res.*



- Atmospheres, 117(D6), <https://doi.org/10.1029/2011JD016978>, 2012.
- 775 Tang, Q., Oki, T., Kanae, S. and Hu, H.: Hydrological Cycles Change in the Yellow River Basin during the Last Half of the Twentieth Century, *J. Clim.*, 21(8), 1790–1806, <https://doi.org/10.1175/2007JCLI1854.1>, 2008.
- United Nations, Department of Economic and Social Affairs and Population Division: World population prospects Data booklet, 2019 revision Data booklet, 2019 revision., 2019.
- 780 USDA and NASS: Farm and ranch irrigation (2008), Special Studies in 2007 Census Publications, United States Department of Agriculture, National Agricultural Statistics Service, AC-07-SS-1. [online] Available from: https://www.nass.usda.gov/Publications/AgCensus/2007/Online_Highlights/Farm_and_Ranch_Irrigation_Survey/fris08.pdf, 2009.
- 785 USDA and NASS: Field Crops, Usual Planting and Harvesting Dates, United States Department of Agriculture - National Agricultural Statistics Service. [online] Available from: <https://downloads.usda.library.cornell.edu/usda-esmis/files/vm40xr56k/dv13zw65p/w9505297d/planting-10-29-2010.pdf> (Accessed 4 July 2019), 2010.
- 790 Verburg, P. H., Dearing, J. A., Dyke, J. G., Leeuw, S. van der, Seitzinger, S., Steffen, W. and Syvitski, J.: Methods and approaches to modelling the Anthropocene, *Glob. Environ. Change*, 39, 328–340, <https://doi.org/10.1016/j.gloenvcha.2015.08.007>, 2016.
- Voirin-Morel, S.: Hydrographical modelling at a regional scale: application to the Adour-Garonne basin, *Toulouse 3.*, 2003.
- 795 Voltaire, A., Decharme, B., Pianezze, J., Lebeaupin Brossier, C., Sevault, F., Seyfried, L., Garnier, V., Bielli, S., Valcke, S., Alias, A., Accensi, M., Arduin, F., Bouin, M.-N., Ducrocq, V., Faroux, S., Giordani, H., Léger, F., Marsaleix, P., Rainaud, R., Redelsperger, J.-L., Richard, E. and Riette, S.: SURFEX v8.0 interface with OASIS3-MCT to couple atmosphere with hydrology, ocean, waves and sea-ice models, from coastal to global scales, *Geosci. Model Dev.*, 10(11), 4207–4227, <https://doi.org/10.5194/gmd-10-4207-2017>, 2017.
- 800



Zaitchik, B. F., Evans, J. and Smith, R. B.: MODIS-Derived Boundary Conditions for a Mesoscale Climate Model: Application to Irrigated Agriculture in the Euphrates Basin, *Mon. Weather Rev.*, 133(6), 1727–1743, <https://doi.org/10.1175/MWR2947.1>, 2005.



Table 1 – Evaluation datasets.

Observations	Source	Reference	Spatial resolution	Time period	Sampling time
Water used for irrigation	USGS	https://waterdata.usgs.gov/ne/nwis/wu	County	1985-2015	5 years
LAI	CGLS	Baret et al., 2013	0.01°	1999-2018	10 days
GPP	FLUXCOM	Jung et al., 2017	0.25°	1980-2013	1 day
Evapotranspiration	GLEAM	Martens et al., 2017	0.25°	2003-2018	1 day
Land surface temperature at 12h	CGLS	Freitas et al., 2013	0.05°	2009-2018	1 day
In situ precipitation	University of Nebraska-Lincoln	http://climod.unl.edu/	local	2009-2012	Monthly



Table 2 – Irrigation parameters.

Symbol	Definition	Default value (this study)
I_T	Irrigation type	sprinkler
I_{NT}	Irrigated nature type	C3 crops, C4 crops, shrubs
I_W	Water amount per irrigation water turn	30 mm
I_D	Irrigation water turn duration	8 hours
SWI_1	SWI threshold for triggering the first water turn	0.70
SWI_2	SWI threshold for triggering the second water turn	0.55
SWI_3	SWI threshold for triggering the third water turn	0.40
SWI_{4+i}	SWI threshold for triggering the following water turns (i, integer > 0)	0.25
Δt_{Wn}	Minimum time lapse between two water turns	7 days
Δt_{WH}	Minimum time lapse between the last water turn and the harvest	15 days
t_E	Emergence date	15 May (± 15 days)
t_H	Harvest date	15 September (± 15 days)



815 **Table 3 – Main set up of the three 40-year evaluation experiments forced by ERA-5 atmospheric variables over Nebraska. Crop phenology is defined by emergence and harvest dates, while irrigation corresponds to additional water supply.**

Experiment	Crop phenology	Irrigation	Forcing	Spinup time	Simulation time period
ISBA_ref	no	no	ERA-5 $0.25^\circ \times 0.25^\circ$	20 years	1979-2018
ISBA_pheno	YES	no			
ISBA_pheno_irr	YES	YES			



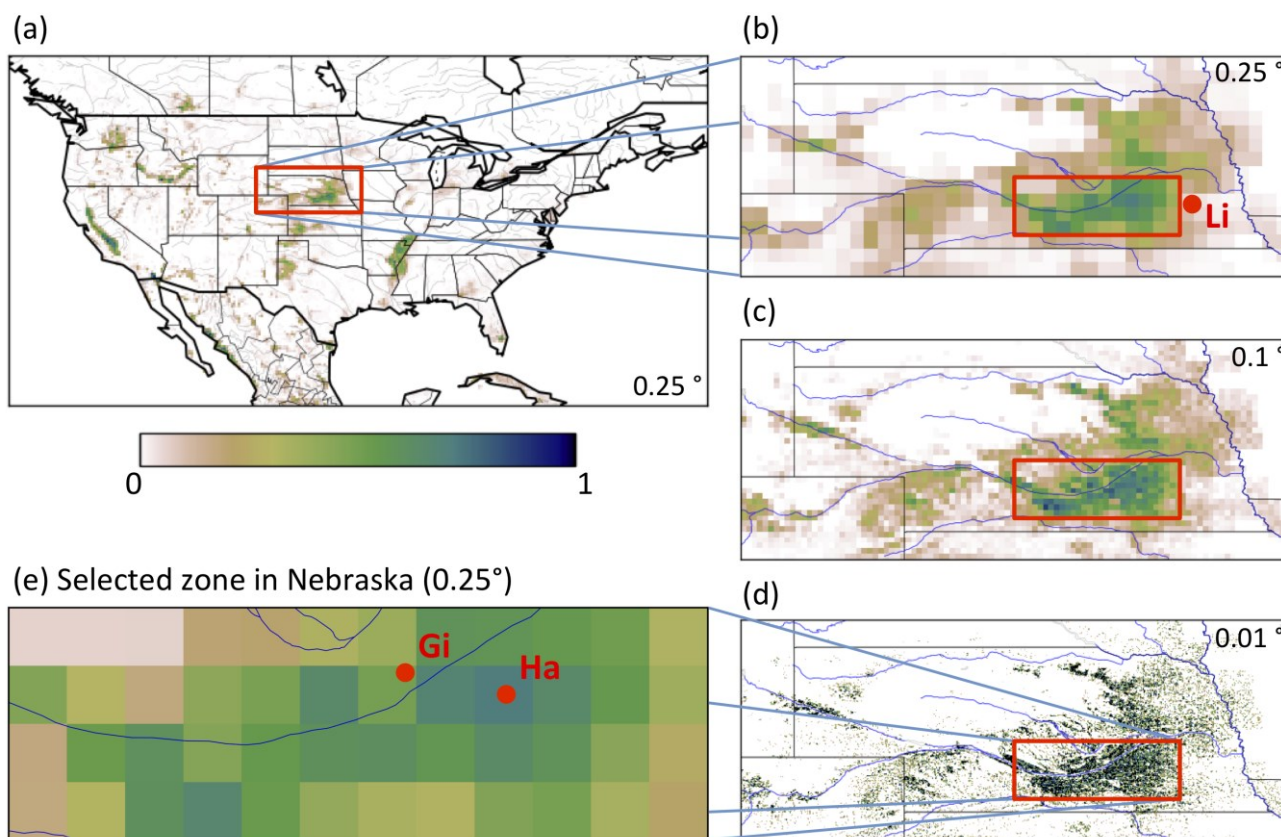
820

Table 4 – Observed and simulated mean LAI peak characteristics over Nebraska for the 1999-2018 time period for crops (see Fig. 4) and all vegetation types (see Fig. 5).

Vegetation types	LAI source	Peak LAI (m ² m ⁻²)	Peak LAI date
Crops	Observations	4.9 (±0.8)	31 July
	ISBA_ref	3.6 (±0.2)	2 July
	ISBA_pheno	3.5 (±0.2)	26 August
	ISBA_pheno_irr	3.7 (±0.1)	28 August
All	Observations	3.8 (±1.5)	31 July
	ISBA_ref	3.3 (±0.3)	1 July
	ISBA_pheno	3.1 (±0.3)	16 July
	ISBA_pheno_irr	3.1 (±0.3)	16 July



825

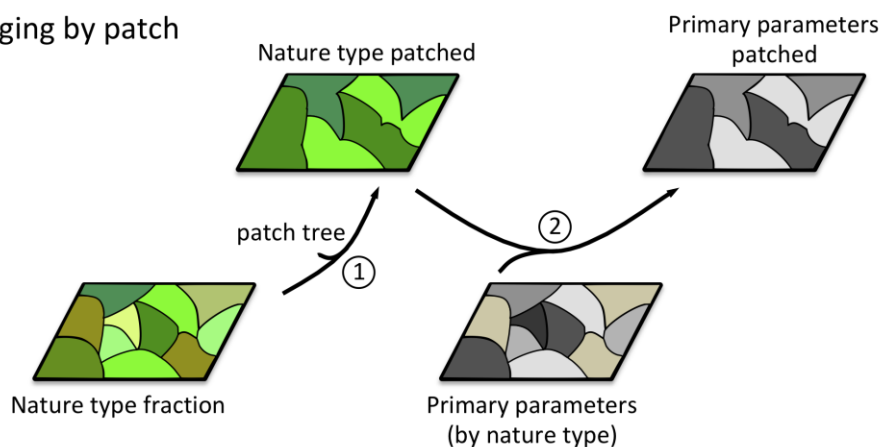


830 **Figure 1 – Irrigation fractional coverage derived from Meier et al. (2018) over (a) the Continental**
United State (CONUS), (b, c, d, e) Nebraska: at (b) $0.25^\circ \times 0.25^\circ$, (c) $0.1^\circ \times 0.1^\circ$, (d) $0.01^\circ \times 0.01^\circ$
spatial resolutions, and (e) over the selected zone in southern Nebraska considered in this study.
The red boxes show the location of the different zooms. The “Li”, “Gi” and “Ha” red dots
correspond to the Lincoln weather station, Grand Island weather station, and Hampton irrigated
area, respectively.

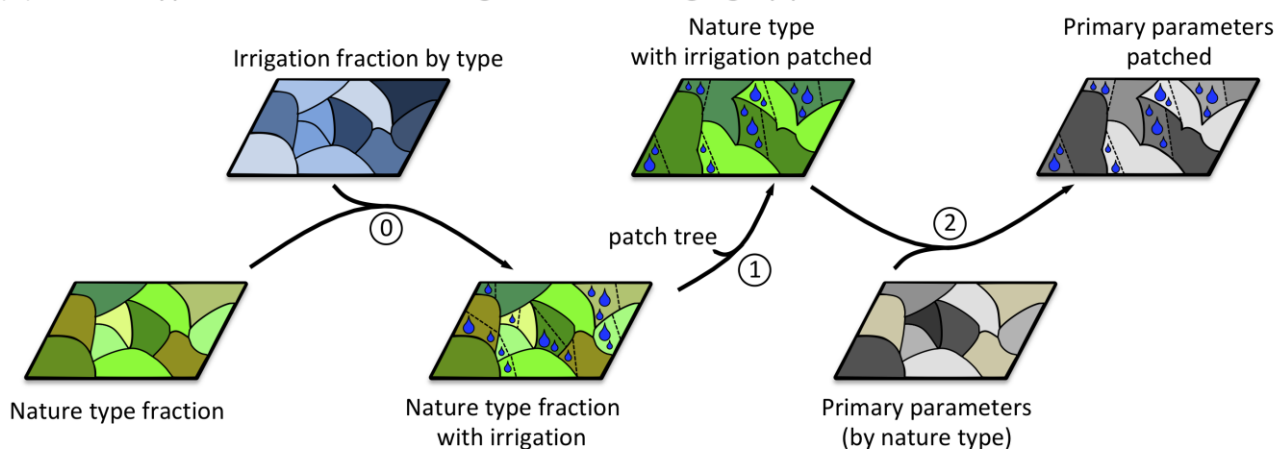
835



(a) Standard nature type merging by patch

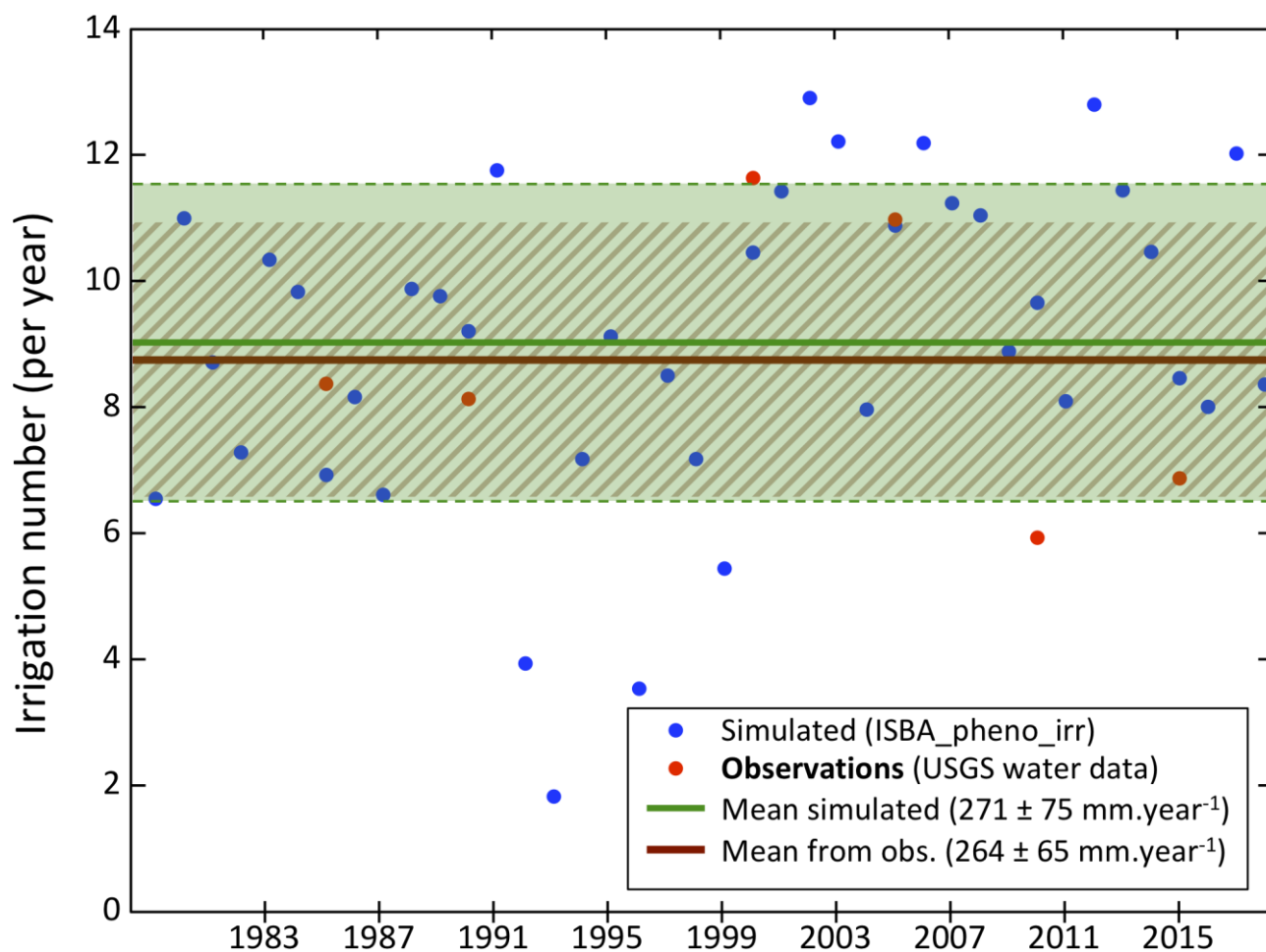


(b) Nature type distributed with irrigation and merging by patch



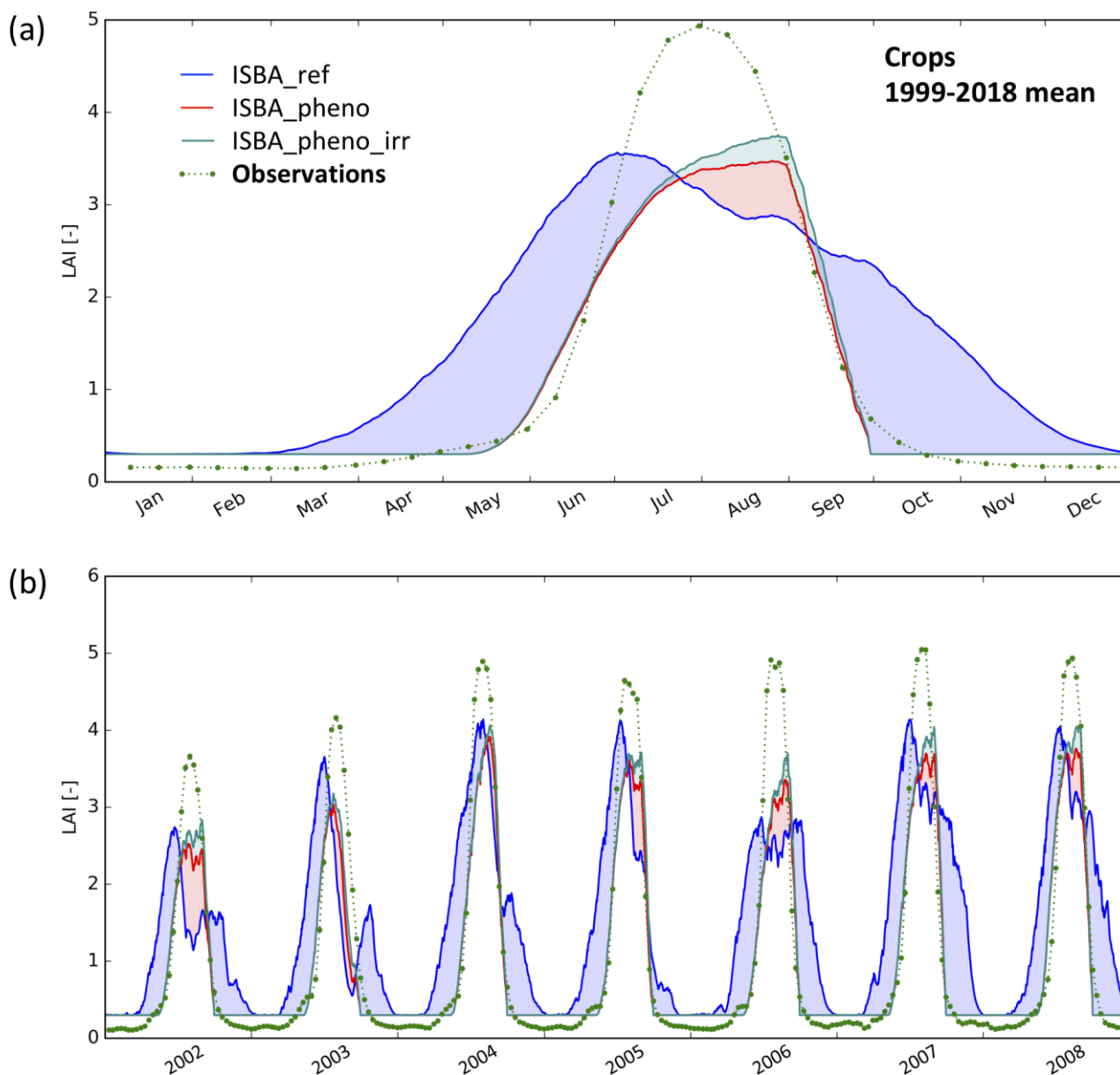
840

Figure 2 – Diagram of the processing steps to obtain the ISBA model primary parameters from the nature types: (a) with the original method and (b) with the new method developed for irrigation. The different steps consist of: (0) cross-referencing the maps of vegetation cover (nature types) and irrigation fractional coverage (addition of irrigated nature type classes where irrigation is possible), (1) merging nature type classes following path aggregation rules (see Fig. S1.1), and (2) computing primary parameter values following the patch fraction map.



845

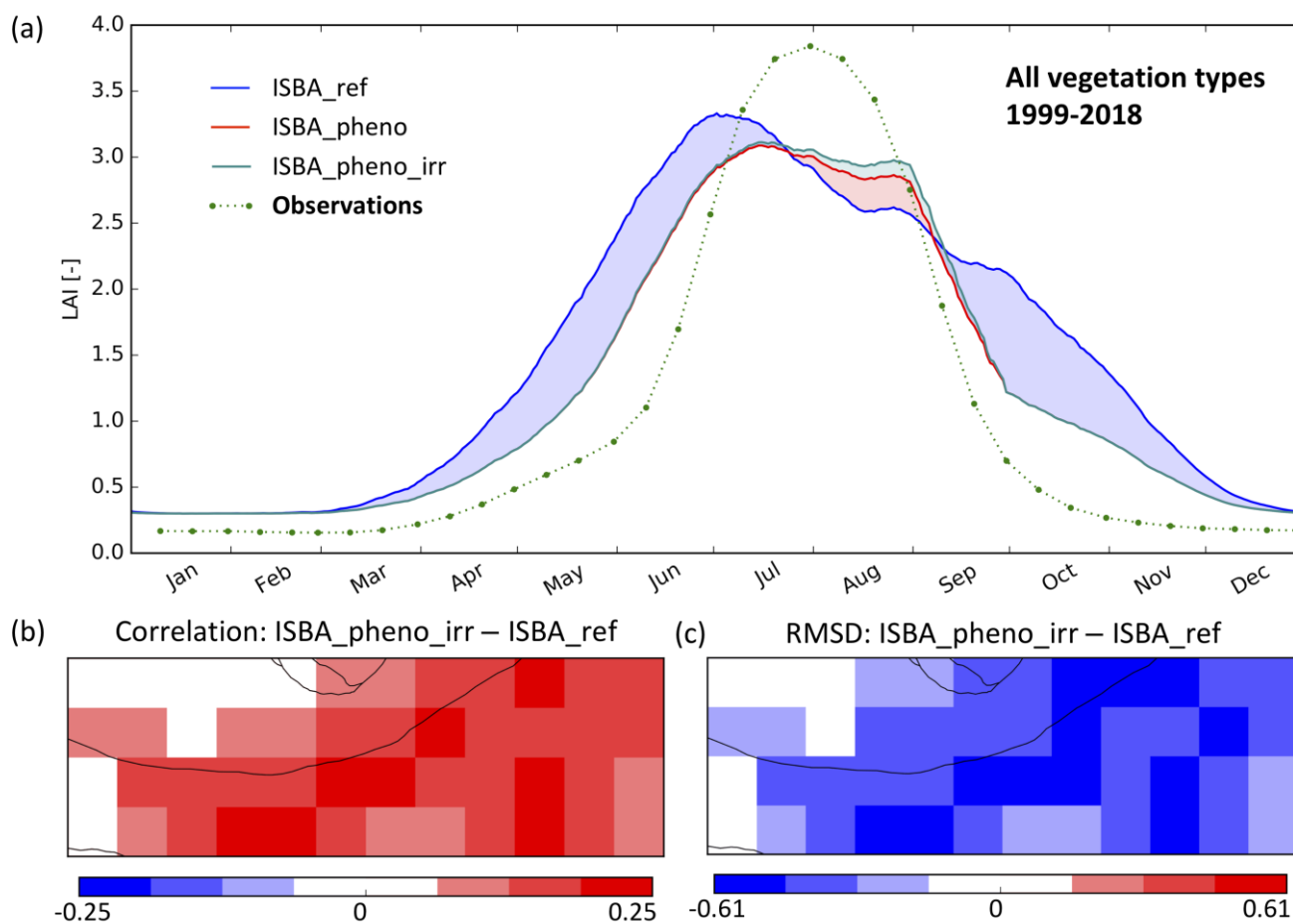
Figure 3 – Yearly cumulated number of irrigation events simulated by the model for the studied area in Nebraska from 1979 to 2018 (blue line). The mean and standard deviation of the yearly values are shown for the model (green solid and dashed lines, respectively), and for the USGS water data from 1985 to 2019 (brown lines).



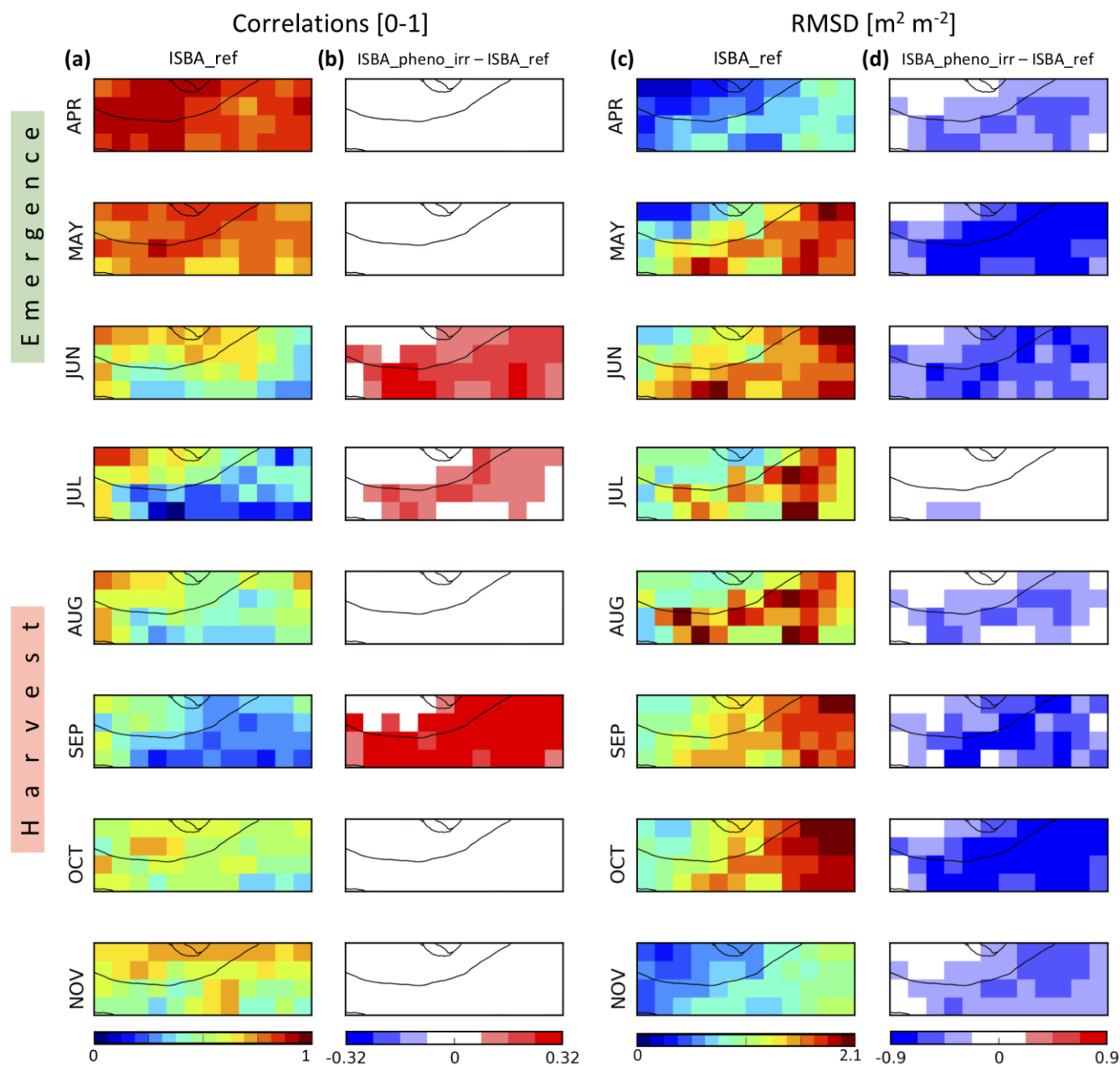
850

Figure 4 – LAI ($\text{m}^2 \text{m}^{-2}$) of irrigated crops (C3 or C4) in the most densely irrigated part of Nebraska (Fig. 1e): (a) seasonal variation for the time period from 1999 to 2018, (b) daily time series from 2002 to 2008. Simulated LAI is shown for the irrigated fraction, from the reference simulation (ISBA_ref, blue line), and from the simulations with only agricultural practices and with agricultural practices and irrigation (ISBA_pheno, red line, and ISBA_pheno_irr, cyan line, respectively). Satellite-derived LAI observations (green dots) are for areas where the fraction of C3 or C4 irrigated crops is larger than 50 %.

855



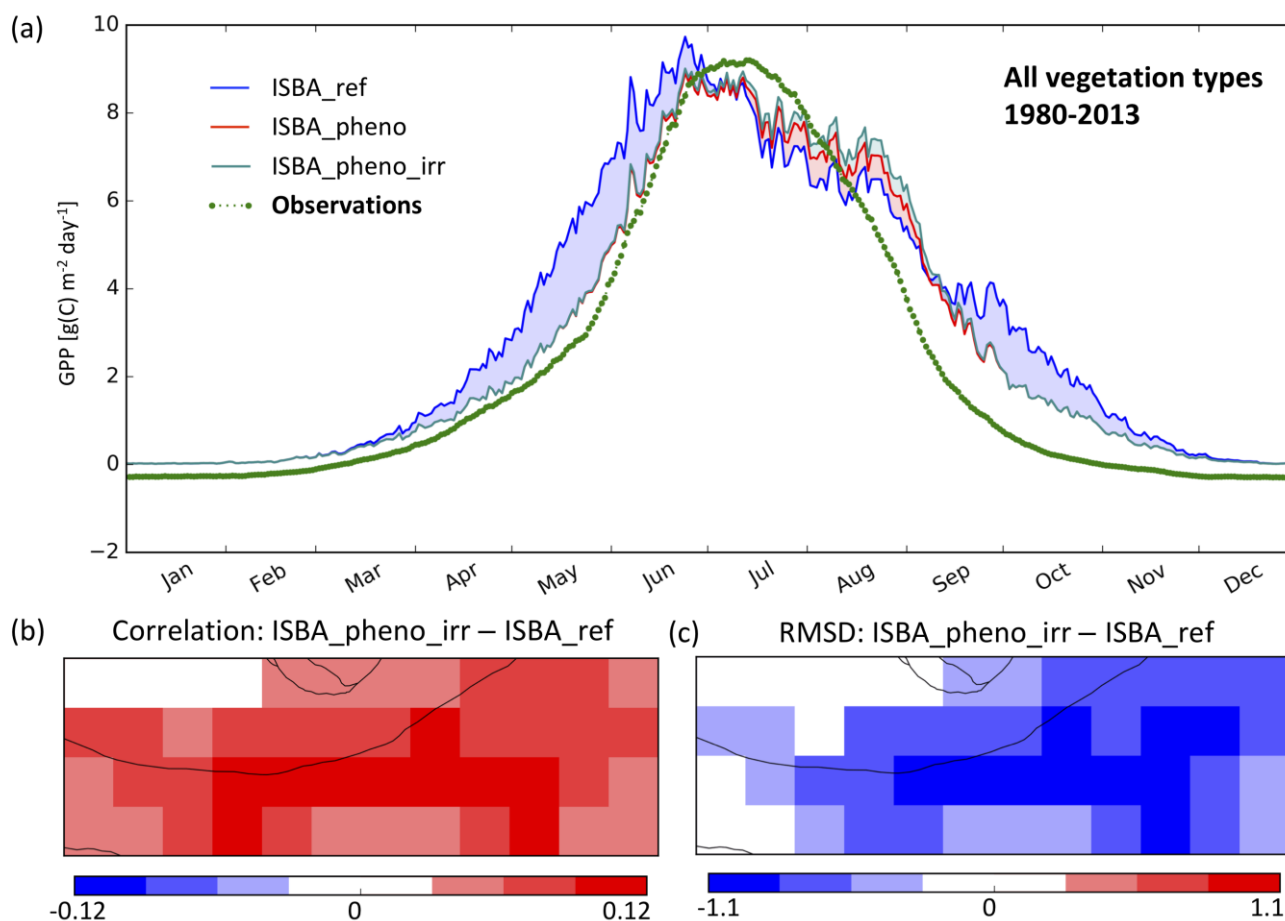
860 **Figure 5 – Simulated vs. observed LAI (m^2m^{-2}) of all vegetation types, in the most densely irrigated part of Nebraska (Fig. 1e) from 1999 to 2018: (a) seasonal variation of mean LAI of ISBA_ref (blue line), ISBA_pheno (red line), ISBA_pheno_irr (cyan) simulations and of satellite-derived observations (green dots), (b) temporal correlation and (c) RMSD score difference maps showing the added value of the ISBA_pheno_irr with respect to ISBA-ref.**



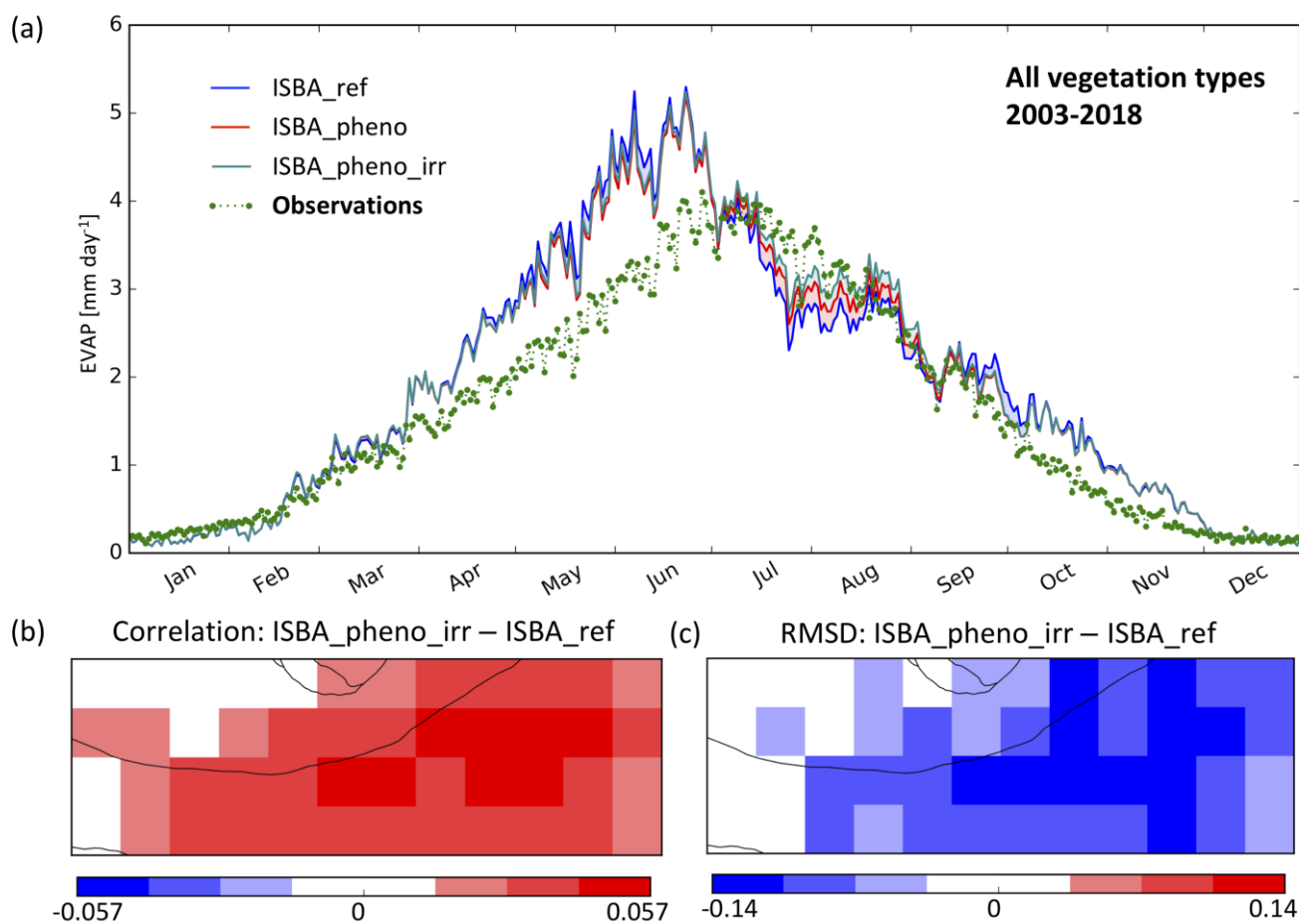
865

Figure 6 – Comparison of simulated LAI with CGLS LAI observations from 1999 to 2018 during the vegetation growing and senescence time period from April to November. Monthly temporal correlation (a, b) and RMSD (c, d) maps are shown for the reference simulation without a representation of irrigation ISBA_ref (a, c). The added value of the ISBA_pheno_irr simulation with respect to ISBA-ref is shown through score difference maps (b, d).

870

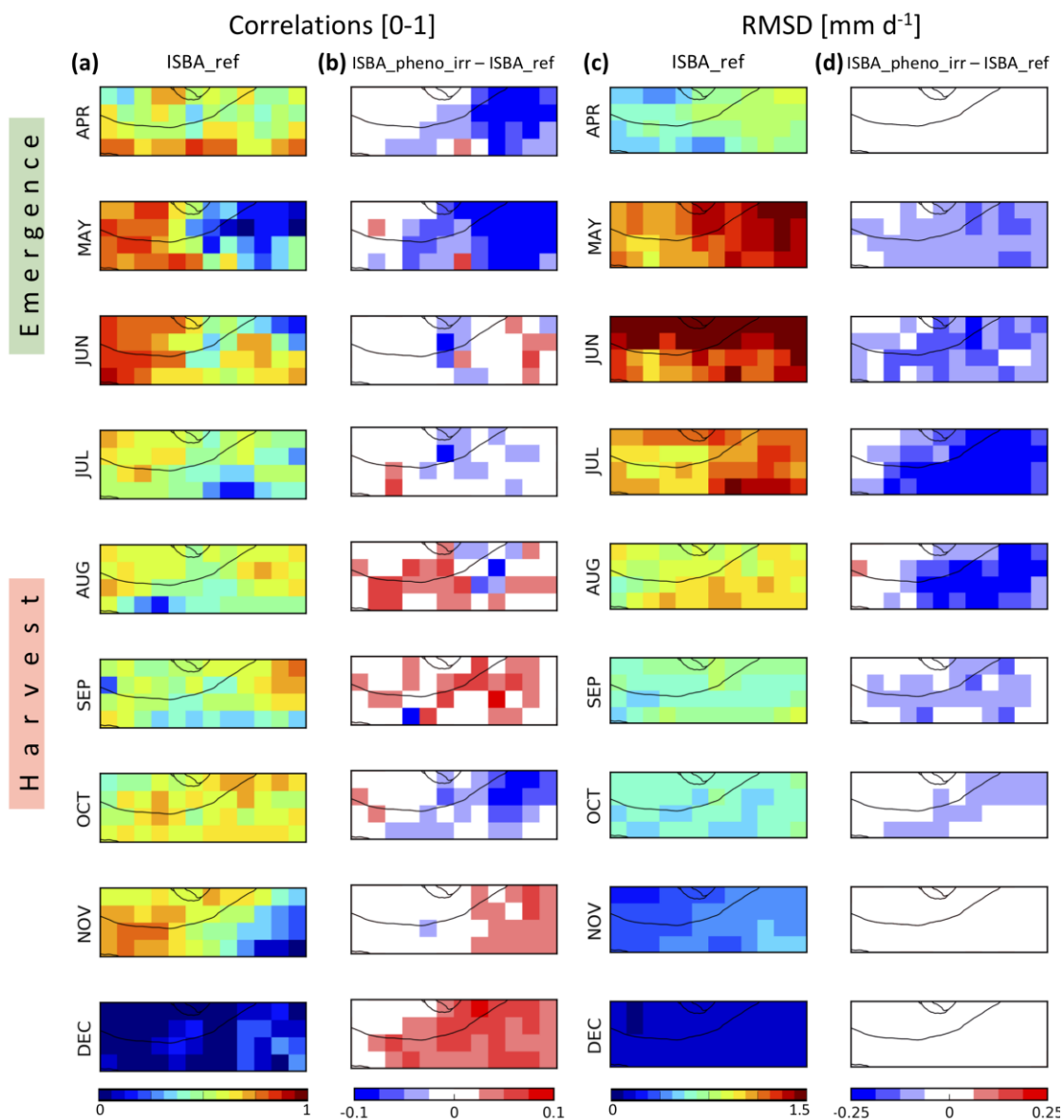


875 **Figure 7 – Seasonal variation of mean daily GPP values (gC m⁻² d⁻¹) from 1980 to 2013 (a) as derived from the reference simulation ISBA_ref (blue line), ISBA_pheno (red line), ISBA_pheno_irr (cyan) and observations (green dotted line). Temporal correlation (b) and RMSD (c) score difference maps show the added value of the ISBA_pheno_irr simulation with respect to ISBA-ref.**



880 **Figure 8 – Seasonal variation of mean daily evapotranspiration values ($\text{kg m}^{-2} \text{d}^{-1}$) from 2003 to 2018 (a) as derived from the reference simulation ISBA_ref (blue line), ISBA_pheno (red line), ISBA_pheno_irr (cyan) and GLEAM observations (green dotted line). Temporal correlation (b) and RMSD (c) score difference maps show the added value of the ISBA_pheno_irr simulation with respect to ISBA-ref.**

885



890 **Figure 9 – Comparison of simulated evapotranspiration with GLEAM evapotranspiration**
observations from 2003 to 2018 during the vegetation growing and senescence time period from
April to November. Monthly temporal correlation (a, b) and RMSD (c, d) maps are shown for the
reference simulation without a representation of irrigation ISBA_ref (a, c). The added value of
the ISBA_pheno_irr simulation with respect to ISBA-ref is shown through score difference maps
(b, d).

895

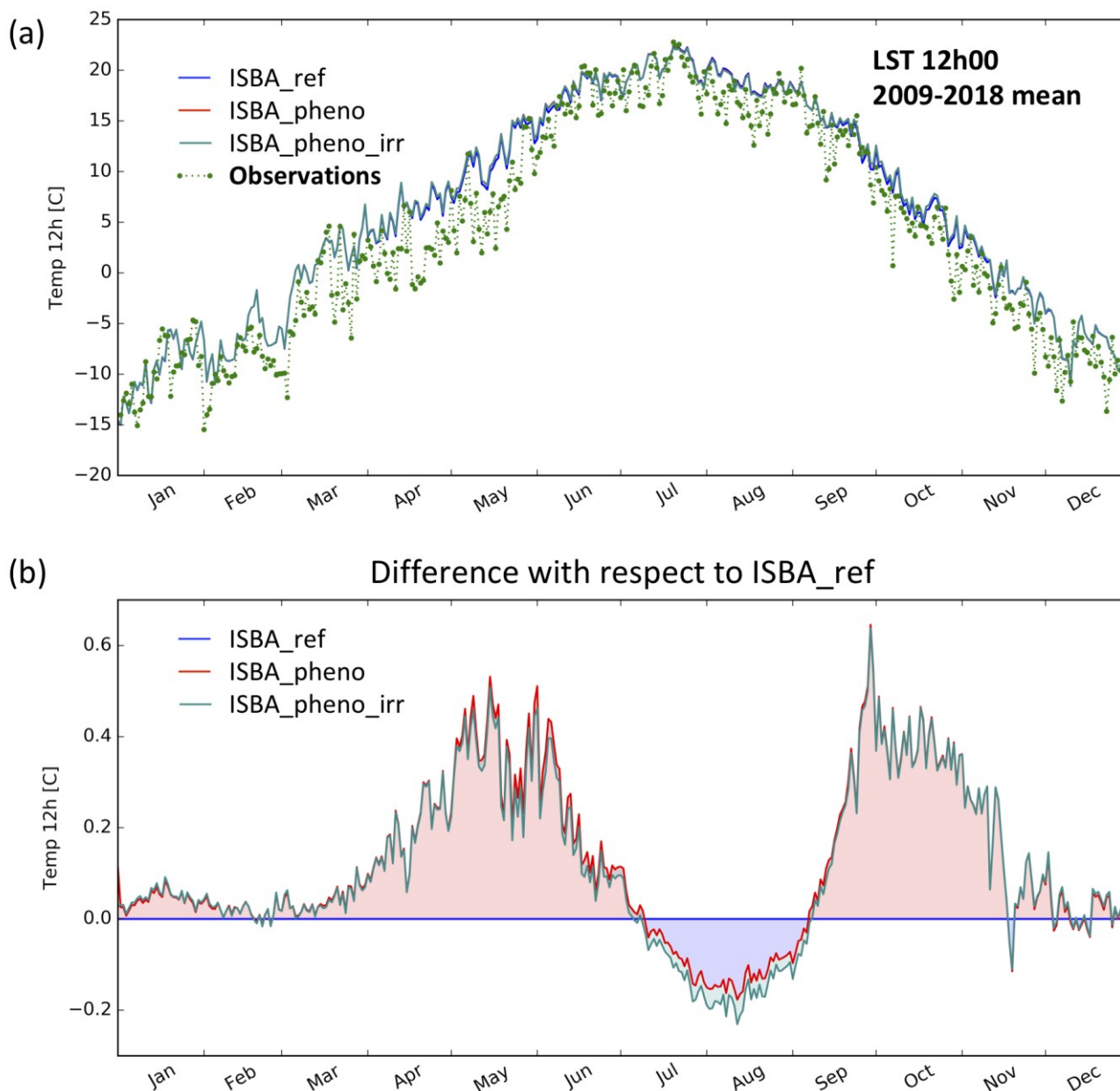
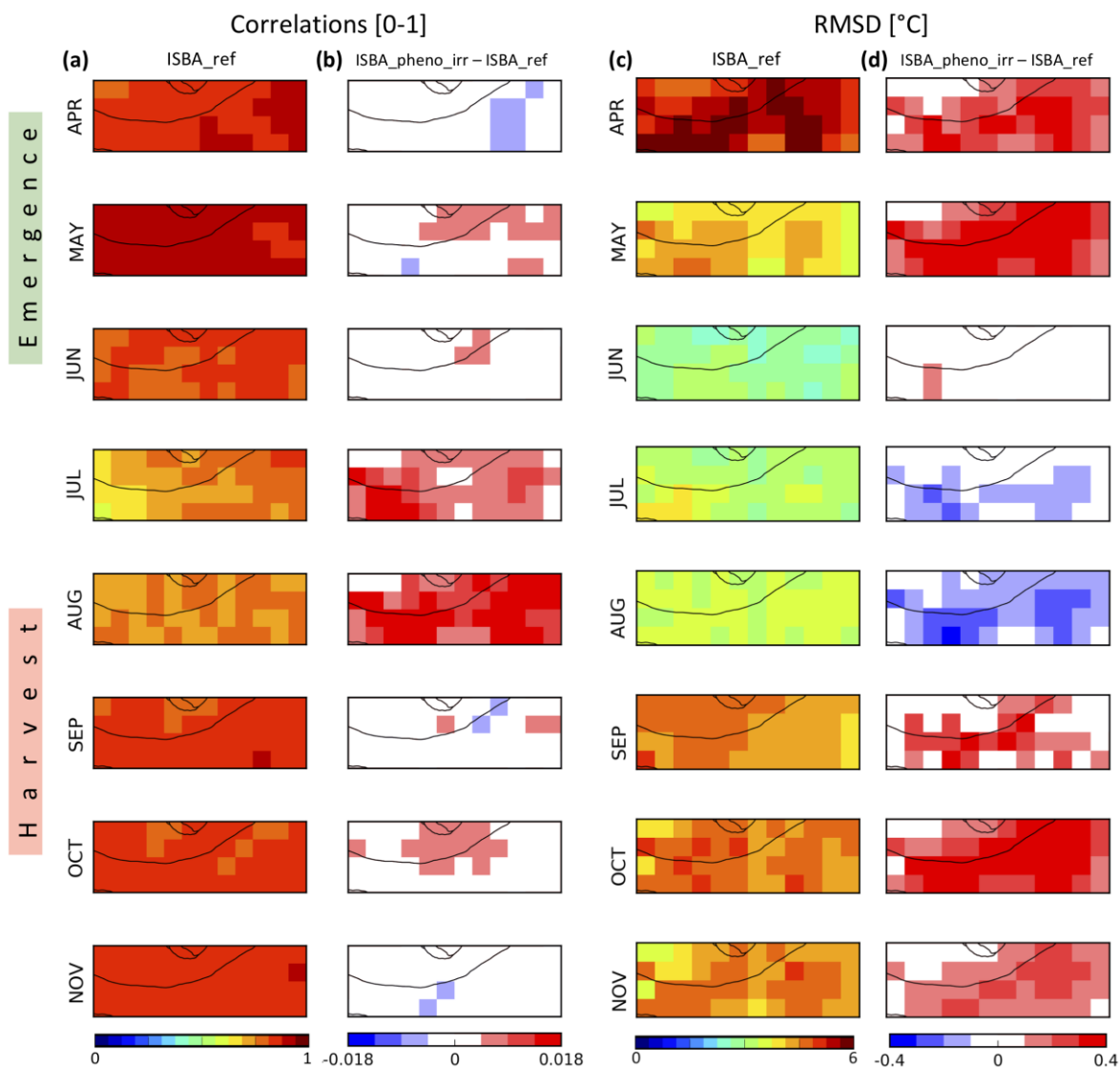


Figure 10 – Seasonal variation of surface temperature daily values at 12:00 local time (degree C) from 2009 to 2018 (a) as derived from the reference simulation ISBA_ref (blue line), ISBA_pheno (red line), ISBA_pheno_irr (cyan) and the CGLS product (green dotted line). The surface temperature differences at 12:00 local time (b) of ISBA_pheno_irr and ISBA_pheno simulations with respect to the ISBA-ref simulations are shown.

900



905 **Figure 11 – Comparison of simulated surface temperature daily values at 12:00 local time with CGLS observations from 2009 to 2018 during the vegetation growing and senescence time period from April to November. Monthly temporal correlation (a, b) and RMSD (c, d) maps are shown for the reference simulation without a representation of irrigation ISBA_ref (a, c). The added value of the ISBA_pheno_irr simulation with respect to ISBA-ref is shown through score**
 910 **difference maps (b, d).**